DIGITAL MODELLING FOR PERFORMANCE PREDICTION OF HYSTERESIS MOTORS

SIDDE GOWDA DEVE GOWDA

DIGITAL MODELLING FOR PERFORMANCE PREDICTION

OF HYSTERESIS MOTORS

by

© Sidde Gowda Deve Gowda, B.E.

A Thesis submitted in partial fulfilment
of the requirements for the degree of
Master of Engineering

Faculty of Engineering and Applied Science
Memorial University of Newfoundland

December 1979

St. John's Newfoundland, Canada

To My Parents

ABSTRACT

The performance prediction of the hysteresis motor depends largely on the success of optimized representation of the actual B-H loop of its rotor hysteresis material. Digital simulation of the typical hysteresis materials like 17% cobalt steel, 36% cobalt steel and Oerstit-70 alloys having coercivity lying between 4 and 20 kA/m and remanent flux density lying between 0.8 and 1.3 T are carried out. The simulation is based on the modified Frölich's approach. Reasonably close agreement is found between the simulated and those supplied by the power magnet manufacturing company.

On the basis of parallelogram approximations analytical models of the circumferential-flux hysteresis motor have been given. The motor field equations are then solved, to predict the terminal quantities, using the digital B-H loop modelling. The air-gap power of the hysteresis motor is studied as a function of coercive force, remanent flux density, saturated relative permeability and unsaturated relative permeability of the hysteresis material. A series of tests were carried out using 17% cobalt steel hysteresis rotor. The reasonably close agreement between the terminal quantities predicted from the digital simulation and those measured experimentally validates the usefulness of digital simulation of the hysteresis motor.

ACKNOWLEDGEMENTS

I wish to express my sincere thanks to Dr. M.A. Rahman, Assoc. Professor of Engineering and Applied Science, Memorial University of Newfoundland, for his guidance, valuable encouragement throughout the research project.

Thanks are due Mr. G.H. Hale for his help during the Experimental work, Miss. Dona Parsons for her valuable help during the Programming period.

I am also thankful to Dean F.A. Aldrich of Faculty of Graduate Studies, for the award of Graduate Fellowship during the period of this study. I am indebted to my wife Yeshoda for her continual support throughout this work.

TABLE OF CONTENTS

Page

LIST OF TABLES

LIST OF FIGURES

Page

GLOSSARY OF SYMBOLS

r_g	: Radius at the Airgap
r_h	: Radius to Centre of Hysteresis Material
g	: Length of Airgap
H	: Magnetic Field Intensity
H_c	: Coercive Force of Hysteresis Material
B	: Flux Density
h	: Radial Thickness of the Hysteresis Material
N_s	: Number of Stator Turns
P	: Number of Poles
B_r	: Residual Flux Density in the Hysteresis Material
$F_{h\theta}$	: Magnetic Potential Drop in The Hysteresis Material
F	: General Symbol for Magnetic Potential
F_θ	: Magnetomotive Force at Angle θ
$F_{0\theta}$	: Magnetic Potential Drop Across R_0
$F_{p\theta}$	: Magnetic Potential Drop Across R_p
$\hat{B}$	: Peak Magnetic Flux Density
ΔF	: Incremental Change in Magnetic Potential
B_h	: Radial Flux Density in Hysteresis Material
H_h	: Magnetic Field Intensity in The Hysteresis Material
l	: Axial Length of Rotor
L_g	: Airgap Inductance
E_p	: R.M.S Voltage of Non-linear Element
E_g	: Airgap Voltage
E_a	: Supply Voltage to The Phase 'a'

R_p : Incremental Reluctance Derived From R_s and R_0

F_q : Maximum Force of $F_{q\theta}$

θ : Radian Angle

ω : Stator Angular Frequency

μ_{rs} : Saturated Relative Permeability

μ_{r0} : Unsaturated Relative Permeability

μ_0 : Permeability of Free Space

m : Number of Phases

s : Slip

R_g : Airgap Reluctance

R_0 : Unsaturated Incremental Reluctance

R_s : Stator Resistance

ϕ_θ : Flux at Angle θ

$\phi_{h\theta}$: Flux Through the Idealized Hysteresis Element at an Angle θ

L_0 : Inductance Dual R_0

L_p : Inductance Dual R_p

R_p : Saturated Incremental Reluctance

$\phi_{p\theta}$: Angular Flux Density Through Square Loop Element

M_s : Saturation Magnetization Intensity

M(a,b) : Critical Intensity of a Preisach-Néel's Elemental Segment(T)

S(a,b) : Distribution Function of Preisach-Neel's ($T.m^2A^2$)

CHAPTER I

INTRODUCTION

1.1 GENERAL OUTLINE

Motor and systems designers have recently taken a long second look at the hysteresis motors' unique characteristics. Its uniform torque, low starting current, and lack of synchronising problems make this type of motor favourable to a number of modern industrial applications. Of all the unique features of a sychronous hysteresis motor, its flat speed-torque characteristics, nearly constant power factor, low noise level and simple rotor construction stand foremost.

The major starting problem which has been inherent in induction machines does not arise at all in case of hysteresis machine, as the resistance of the hysteresis rotor is ideally a direct function of the slip. The hysteresis machine can accelerate all the load that it can carry to synchronous speed irrespective of the load inertia, as it possess inherent built-in constant synchronising torque, unlike an induction machine. In comparision to induction or synchronous motors, it has almost no stability problem. The hysteresis motor is a type of synchronous motor that once was thought of limited usefulness. Development in permanent magnet materials having more hysteresis energy per unit volume like Alnico-5, Simonds 81, Oerstit-70, P6-alloy, Vically and cobalt steel alloys etc., have led to the production of hysteresis motors in fractional horsepower range, which has got intensive applications as drive motors in clocks, recording equipments, gyros, computer tape-drives and in general where constant torque, speed and quiet operations are required. Its starting and accelerating current is low in order of about 150 percent of full-load current requirement.

Apart from the above mentioned merits, it has also a number of demerits, such as low power factor, high magnetising current, and low efficiency associated with high parasitic losses in its rotor magnetic material. Therefore the use of hysteresis motors have been limited to certain special fields where efficiency might not count so much.

In recent years the development of new and improved designs of small and medium-sized brushless synchronous motors are gaining momentum [1]. In part, this is due to a changing market for synchronous a.c. drives and development in power electronics. The combination of inverter and synchronous motors has distinct advantages [2-6] over other forms of drive for applications requiring precise speed combined with smooth starting capability, constant torque and noiseless operation. For this type of applications hysteresis motors are now widely used along with others, particularly reluctance and a.c. permanent magnet types.

The foremost thing to consider seriously in the design of electrical equipment and machinery is to minimise the hysteresis and eddy current losses as they are detrimental to the efficiency and performance. However, in the case of the hysteresis machine 'hard' magnetic materials are used, which are usually not conducive to lamination. The word 'soft' and 'hard' meant low and high coercive force materials respectively.

1.2 CONSTRUCTION

A hysteresis motor has no winding on the rotor. Generally, it exhibits substantially constant torque from stand still to synchronous speed. Its special characteristics result from the hard magnetic material of which the rotor is made and simple rotor construction. The cross-section of the Hysteresis machine is shown in the Fig. (2.1). Unlike other synchronous motors, the hysteresis motor has a perfectly round and symmetrical rotor. That means that the rotor has no salient poles. Hence it has no preferred position for synchronising. In its simple form, it has a conventional slotted and laminated stator with phase windings and a homogeneous cast sleeve (in the present work 17% cobalt steel is used) of permanent magnet material comprising active part of the rotor. The active sleeve is secured to the shaft over a non-magnetic support. (in the present work aluminium sleeve is used).

1.3 OPERATION

The hysteresis characteristic of its rotor magnetic material is the main cause for the development of the driving torque. Hence the name is hysteresis motor. The principle of developing its fundamental driving torque is quite simple. When an alternating voltage is impressed acrosss the stator terminals, the alternating currents establish a rotating field in the rotor, which causes the flux density to lag behind the magnetic intensity due to the hysteresis phenomena of its magnetic material. The angle by which the flux density lags the magnetic intensity is termed as hysteresis lag angle. The phase angle between the stator magnetomotive force and the resultant airgap flux density gives rise to the driving torque. Lag angle depends only on the area of hysteresis loop of the rotor magnet and independent of the frequency of magnetisation neglecting eddy currents.

Since the driving torque is directly proportional to the area of the loop, the developed torque in the hysteresis motor is the same all the way from zero to synchronous speed. At synchronous speed the operation of the motor is accomplished exclusively by the hysteresis torque, as the eddy current torque due to the main fundamental field is zero. In a hysteresis motor, when the rotor is locked and the stator field is rotating, the flux density at any point in the rotor follows a major hysteresis loop, with a frequency equal to the stator supply frequency. When the motor is accelerating to the synchronous speed, the rotor field moves backward at a diminishing rate with respect to the rotating field produced by the stator. At any one point on the rotor, the frequency of the hysteresis loop decreases because of the decrease of slip, until at synchronous speed, when the hysteresis cycle completely stops. At the synchronous speed the rotor develops magnetic poles similar to the d.c. excited synchronous motor. The magnetic potential and flux density waves are no longer moving relative to the rotor, as it attains its synchronism. Thus the rotor containing permanent magnet material and rotating at synchronous speed will have fundamental waves of the flux and magnetomotive force tied to it . Each element of the rotor ceases to operate cyclically on major B-H loop, and carries a constant flux density.

For sinusoidal revolving mmf, the airgap flux density wave is distinctly non-sinusoidal, because of the hysteresis nature of the rotor magnetic material. This has been illustrated in the Fig. (1.1) for

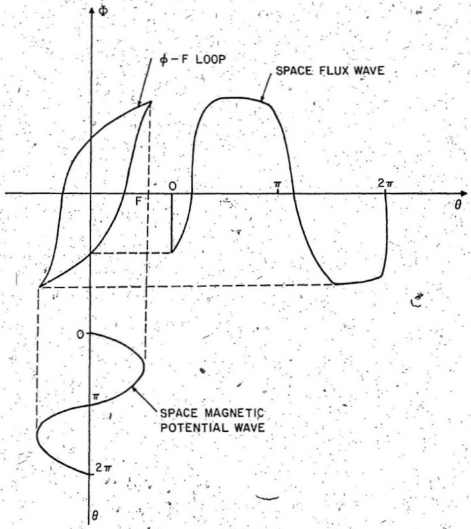

FIG. 1.1 FLUX DISTRIBUTION AROUND HYSTERESIS ROTOR FOR SINUSOIDAL MMF WAVE

the hysteresis machine [7]. Thus at synchronous mode of operation the rotor does not experience any time varying effects of harmonics present in the non-sinusoidal flux wave.

1.4 LITERATURE REVIEW

The hysteresis motor was first explored as a torque producing device by Steinmetz [9] in 1908. He was the pioneer who put a stepping stone to the world of hysteresis machine. The next major contribution was by Teare [10] in 1940, who showed a method of calculating the torque from known field configuration of magnetic flux and magnetomotive force in the hysteresis material of the rotor, on the assumption of sinusoidally revolving stator mmf. Further research was carried out by Roters [11] on the theory of development of torque from both hysteresis lag angle and from total loop energy points of view. Finally, Roters showed that parasitic losses which occur in the rotor, influenced by the local flux oscillations could be greatly reduced by designing the stator with closed slots. This opened the gate for the practical hysteresis motors in fractional horse power range.

In the analyses [10, 11] the effect of eddy currents flowing in the rotor magnetic material on the air-gap field was neglected. Because of the peculiar shape of the magnetic hysteresis loop of the rotor, there remained a major problem in predicting the equivalent magnetic or dual electric equivalent parameters of it. Hence the foremost problem in the analysis of a hysteresis machine was the treatment of the hysteresis loop of the rotor magnetic material. The analysis of the hysteresis machine based on the actual hysteresis loop becomes almost a prohibitive due to its property of non-linearity. Lot of research [7-14, 21-23, 25] have been undertaken to approximate the hysteresis loop so as to facilitate the formulation of equations in its analysis.

Teare [10] was the pioneer who made such an approximation in his analysis of motor. He replaced the actual hysteresis loop by means of an inclined ellipse, which has almost the same maximum values of B and H. The elliptical representation was further extended by Roters [11] and Robertson [12] for fractional horsepower hysteresis motor. Miyari and Kakaoka [13] extended the elliptical representation still further neglecting the space harmonics in both the stator mmf and the airgap flux density waves. They assumed the permeability of the rotor hysteresis ring to be finite and neglected the eddy currents flowing in the magnetic ring. Following Miyari and Kakaoka's, O'Kelly [14] analysed the hysteresis motor by the equivalent Kron primitive machine, in which the rotor hysteresis material was replaced by closed coils with self reactance being assumed equal to mutual reactance. However, it is claimed that the rotor reactance is better represented in parallelogram approximations developed by Copeland and Slemon [7], in the analyses of radial flux hysteresis machine. The same authors continued their research further and gave a very good account of the analysis of the circumferential-flux type rotor [8]. The flux density distribution in the machine is found [8], using a parallelogram loop approximation to the B-H characteristics of the hysteresis material. An equivalent circuit of the motor was developed.

Copeland and Slemon [7, 8] used the parallelogram method to model the hysteresis loop and predicted the rotor parameters and hence the internally developed torque of the machine in terms of the permeabilities and hysteresis lag angle of the rotor material. Fig. (1.2) shows a parallelogram model. The parallelogram loop model was analysed further by neglecting the rotor eddy currents field effects due to space harmonics on the air-gap field at the synchronous mode of operation. Later in 1969 Rahman, Copeland and Slemon [21] developed expressions to predict the parasitic losses in terms of the air-gap field, the stator current and rotor hysteresis material characteristics.

However the analyses were limited to synchronous mode of operation only. The general analytical models for polyphase hysteresis motor at both synchronous and subsynchronous speeds were developed [15]. Steady-state equivalent circuit models were developed using the parallelogram approximation for both synchronous and subsynchronous modes of operation. The parasitic losses associated with the rotor hysteresis material, the stator iron loss and saturation effects are best represented by suitable parameters in the general equivalent circuit model [15]. The Preisach-Neel's model has been illustrated in Appendix A.

Experiences with miniature motors gave the impressions that low efficiency and low power factor are the inherent characteristics of the hysteresis motors, making large ratings of such motors impractical. Integral horsepower hysteresis motors with improved efficiency have been built successfully [15-17]. Using "Scaling Techniques", the performances of large motors were studied [18, 19], and it was found that very encouraging results in terms of efficiency and power could be obtained for larger ratings.

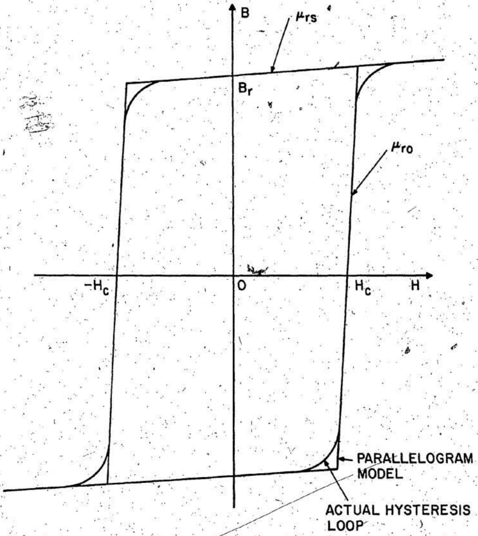

FIG. 1.2 MODELLING OF HYSTERESIS LOOP BY PARALLELOGRAM

1.5 SCOPE

The scope of the present research lies in the computer simulation of B-H loop for low-coercivity permanent magnet materials that are most suitable for the rotor of a hysteresis motor, having coercivity between 0.8 and 1.3 T and to compare with the actual B-H loop available, supplied by the permanent magnet manufacturing company. Based on the computer simulation the motor field equations are solved and the terminal properties of the machine are predicted. Experiments are carried out using hysteresis rotor made of 17% cobalt steel to verify the validity of digital models.

1.6 BRIEF OUTLINE ON THE REMAINING CHAPTERS

Chapter II presents the analysis of the hysteresis machine based on Copeland and Slemon's model.

Chapter III describes the various methods of modelling B-H loop and their adoptability to study the performance of hysteresis motor.

In Chapter IV an attempt is made to simulate the B-H loop of various magnetic materials suitable for rotor of hysteresis motor.

Chapter V presents a method of representing hysteresis which includes the effect of minor loops and computer solution to find the terminal quantities of the hysteresis motor by the digital simulation method.

In Chapter VI, test results of the performance of the hysteresis motor using 17% cobalt steel rotor is given.

Conclusions of the research are presented in Chapter VII. This concluding Chapter also contains suggestions for the work in future.

CHAPTER II

ANALYTICAL MODEL

2.1 INTRODUCTION

The aim of this chapter is to analyse the circumferential flux hysteresis machine with the help of rectangular loop approximation to the B – H characteristic of the hysteresis material. The flux density distribution is found and also the equivalent circuit is developed. Improvement over the rectangular approximation is also carried out. Two approximations are carried out for the B-H model.

2.2 THE CIRCUMFERENTIAL FLUX HYSTERESIS MACHINE

Fig. (2.1) shows a cross – section of a hysteresis machine with a circumferential – flux rotor. The stator is considered to have an m – phase 2 – pole winding each phase of which has its turns sinusoidally distributed in a large number of slots. Unlike in the case of radial flux machine, the flux density after crossing the air-gap radially, must be directed circumferentially around the hysteresis material to complete its path.

The flux distribution in the hysteresis ring is shown in the Fig. (2.2), where the magnetic path is radial in the air gap and circumferential in the hysteresis material. It is assumed that the flux distribution is uniform inside the ring and there is no flux penetration into the non – magnetic sleeve.

The turns N_s of phase 'a' are assumed to be distributed

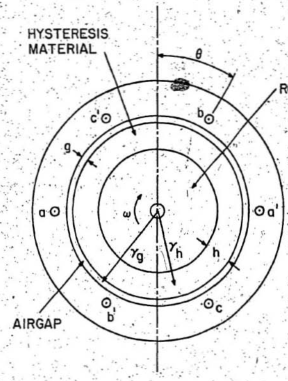

FIG. 2.1 CROSS-SECTION OF CIRCUMFERENTIAL-FLUX HYSTERESIS MACHINE

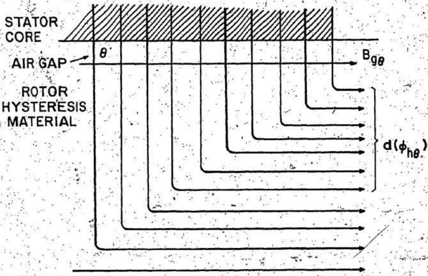

FIG. 2.2 FLUX PATTERNS IN AIRGAP AND HYSTERESIS RING

with a conductor density of

$$Na = \frac{Ns}{2} \; |\sin\theta| \text{ Conductors per radian} \quad . \; . \; . \; (2.1)$$

Let the currents in phase a be expressed in the form of the following equation :

$$i_a = \hat{I} \sin \omega t \text{ amperes} \quad . \; . \; . \; . \; . \; . \; . \; . \; . \; . \; . \; (2.2)$$

and let the stator currents form a balanced polyphase set of sequence a, b, c. Consider the incremental sector of the machine shown in Fig. 2.3. Proceeding clockwise around the path shown, the magnetomotive force of the enclosed conductor is

$$\Delta F = - \frac{mNs\hat{I}}{4} \cos (\omega t - \theta)\Delta\theta \quad \text{amperes} \; . \; . \; . \; (2.3)$$

Assuming that the stator iron has essentially infinite permeability, the incremental mmf of equation 2.3 is absorbed in producing the difference in air-gap flux density at $\theta+\Delta\theta$ ~~with respect to θ and~~ in magnetic field intensity $H_{h\theta}$ of the hysteresis material. Thus,

$$\Delta F = \frac{g}{\mu_o} \left[B_g(\theta+\Delta\theta) - B_{g\theta} \right] - H_{h\theta} \, r_h \Delta\theta . \; (2.4)$$

Equations 2.3 and 2.4 may be combined to give the differential equation

$$\frac{g}{\mu_0} \frac{dB_{g\theta}}{d\theta} = H_{h\theta} \, r_h - \frac{mN_s\hat{I}}{4} \cos (\omega t - \theta) \; . \; . \; . \; . \; . \; . \; . \; . \; . \; (2.5)$$

At this stage, it is assumed that the properties of the hysteresis material can be represented by the ideal rectangular loop as shown in Fig. (2.4). In this idealisation, the flux density B_h in the hysteresis material can increase only with the field intensity H_h is equal to the coercive force H_c and can decrease only when

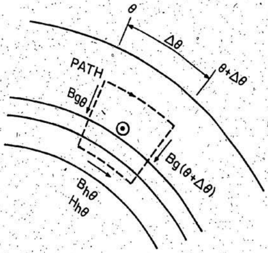

FIG. 2.3 INCREMENTAL SECTION OF MACHINE, SHOWING POSITIVE DIRECTION OF FLUX DENSITY AND FIELD INTENSITY VECTORS

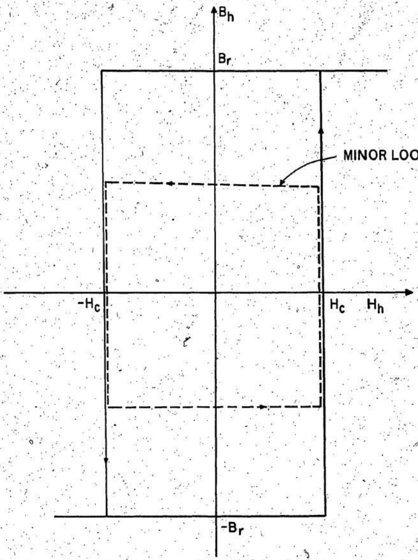

FIG. 2.4 IDEALIZED MAGNETIZATION CHARACTERISTIC FOR HYSTERESIS MATERIAL

$H_h = -H_c$. Let K be a measure of the stator current in per unit of the stator current required to produce coercive force:

$$K = \frac{mN_s\hat{I}}{4r_hH_c} \quad \ldots \ldots \ldots \ldots \quad (2.6)$$

For K > 1, there will be a part of the hysteresis material for which $H_{h\theta} = H_c$. For this part, equation 2.5 can be written as

$$\frac{dB_{g\theta}}{d\theta} = \frac{\mu_0 r_h H_c}{g}\left[1 - K\cos\ (\omega t - \theta\ )\right] \ldots \ldots \quad (2.7)$$

This equation has a solution of the form

$$B_{g\theta} = \frac{\mu_0 r_h H_c}{g}\left[\theta + K\sin\ (\ \omega\ t - \theta\ ) + C\right] \text{webers per meter}^2 \quad (2.8)$$

where C is a constant

The range of application of equation (2.8) and the value of the constant C must now be determined. Since positive coercive force exists over this region, it follows that the flux density in the material encompassed is increasing with time;

$$\frac{dB_{h\theta}}{dt} \geq 0 \quad \ldots \ldots \ldots \ldots \quad (2.9)$$

Throughout this range, the operating point for material is on the right - hand vertical side of the characteristic of Fig. (2.4). The magnetic field in the machine rotates clock wise in Fig. (2.1) with respect to the rotor at subsynchronous rotor speeds. The flux density $B_{h\theta}$ in the material, therefore, will reach a maximum positive value at that point where the rate of application of mmf is reduced to the value which is just sufficient to maintain coercive force. From equations (2.5) and (2.6), this particular condition occurs at the following position:

$$\alpha = \omega t - \theta = \cos^{-1}\frac{1}{K} \quad \ldots\ldots\ldots\ldots (2.10)$$

For the continuity of flux in the machine, the air-gap flux per unit of angle θ must equal the rate of change of flux with θ in the hysteresis material. Thus the following relationship is established:

$$h\,\frac{dB_{h\theta}}{d\theta} = r_g B_{g\theta} \quad \ldots\ldots\ldots\ldots (2.11)$$

Since $dB_{h\theta}/d\theta \geq 0$ over the range of equation (2.8) and since $B_{h\theta}$ is a function of ($\omega t - \theta$), the result is $dB_{h\theta} / d\theta \leq 0$. From equation 2.11, the flux density $B_{g\theta}$ is, therefore, negative. At $\omega t - \theta = \alpha$, then B_{g_θ} must be zero. Equation (2.8), consequently becomes

$$B_{g_\theta} = \frac{\mu_0 r_h H_c}{g}\left[\theta + K\sin(\omega t - \theta) - (\omega t - \alpha) - K\sin\alpha\right] \ldots (2.12)$$

The other limit of range of application for equation (2.12) occurs at ($\omega t - \theta$) $= \delta$ where B_{g_θ} again reaches zero. This value may be determined by iterative solution of equation (2.12) equated to zero:

$$K\sin\delta - \delta = \sqrt{K^2 - 1} - \cos^{-1}\frac{1}{K} \quad \ldots\ldots\ldots (2.13)$$

for values of K.

Because of the symmetry of the machine, there is a similar range in which $H_{h\theta} = -H_c$, and

$$B_{g_\theta} = \frac{\mu_0 r_h H_c}{g}\left[-\theta + K\sin(\omega t - \theta) + (\omega t - \alpha - \pi) + K\sin\alpha\right] \ldots (2.14)$$

Fig. (2.5) shows B_{g_θ} as a function of θ at $t = 0$ for one specific value of K. Between the two parts of the solution given by equations (2.12) and (2.14), the air- gap flux density

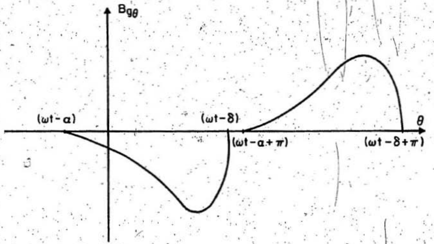

FIG. 2.5 AIR GAP FLUX DENSITY AS A FUNCTION OF θ AT $t=0$ AND $K<1.862$

is equal to zero.

Equations (2.12) and (2.14) give the solution for values of K from 1.0 to the value for which $\delta - \alpha = \pi$. Substituting into equations (2.13) and (2.10) shows that this condition obtains at $K = K_c$ where

$$K_c = \left[\left(\frac{\pi}{2} \right)^2 + 1 \right]^{1/2} = 1.862 \quad \ldots\ldots \quad (2.15)$$

At this value of K, $\alpha = 57.5$ degrees.

For operation with $K > K_c$, the solution of equation (2.8) still applies for the half of the machine in which positive coercive force exists. The constant C must, however, be re-evaluated by setting $B_{g\theta} = 0$ in equation (2.8) for $\theta = \omega t - \alpha$ and $\theta = \omega t - \alpha + \Pi$. Solution of two resultant equations gives

$$\alpha = \sin^{-1} \left(\frac{\pi}{2K} \right) \quad \ldots\ldots\ldots\ldots \quad (2.16)$$

and

$$C = -\omega t - \frac{\pi}{2} + \sin^{-1} \frac{\pi}{2K} \quad \ldots\ldots \quad (2.17)$$

The constant for the region of negative coercive force may be evaluated in a similar manner.

To facilitate determination of the flux linkage of the stator winding, let the air- gap flux density $B_{g\theta}$ be expressed as a Fourier series in σ , where

$$\sigma = \omega t - \theta \quad \ldots\ldots\ldots\ldots\ldots\ldots \quad (2.18)$$

For the range $0<K<1.862$, using equations (2.12) and (2.18) it can be shown that

$$B_{g\theta} = \frac{2}{\pi} \frac{\mu_0 r_h H_c}{g} \left\{ \left[\int_{\alpha}^{\delta} \left(-\sigma + K \sin \sigma + \cos^{-1} \frac{1}{K} - \sqrt{K^2 - 1} \right) \sin\sigma \, d\sigma \right] \sin \sigma \right.$$

$$+\left[\int_{\alpha}^{\delta}\left(-\sigma+K\sin\sigma+\cos^{-1}\frac{1}{K}-\sqrt{K^2-1}\right)\cos\sigma\,d\sigma\right]\cos\sigma\Bigg\}$$

+ higher odd harmonic terms

$$=\frac{2}{\pi}\frac{\mu_0 r_h H_c}{g}\Bigg\{\frac{1}{2}\left[-\frac{\sqrt{K^2-1}}{K}-\frac{K\delta}{1}+\frac{K\alpha}{1}+2\sin\delta+2\cos\delta\left(\frac{K\sin\delta}{2}-\delta+\alpha-\sqrt{K^2-1}\right)\right]\sin\sigma$$

$$+\frac{1}{2}\left[-2\sin\delta\left(\delta+\sqrt{K^2-1}-\alpha\right)-2\cos\delta-\frac{K}{2}\cos 2\delta+\frac{K}{2}\cos 2\alpha+2K\right]\cos\sigma\Bigg\}+$$

+higher odd harmonic terms

$$=\frac{1}{\pi}\frac{\mu_0 r_h H_c}{g}\Bigg\{\left[-\frac{\sqrt{K^2-1}}{K}-K\left(\delta-\alpha\right)+2\sin\delta+2\cos\delta\left(\frac{K\sin\delta}{2}-\right.\right.$$

$$\left.\left.\delta+\alpha-\sqrt{K^2-1}\right)\right]\sin\sigma+\left[-2\sin\delta\left(\delta-\alpha+\sqrt{K^2-1}\right)-2\cos\delta\right.$$

$$\left.-\frac{K}{2}\left(\cos 2\delta-\cos 2\alpha\right)+2K\right]\cos\sigma\Bigg\}$$

+ higher odd harmonic terms

Neglecting the higher harmonic terms, the R.H.S. of the above equation is of the type

$$A\cos\sigma+B\sin\sigma=J\sin\beta \quad \ldots\ldots\ldots\ldots\ (2.19)$$

Where

$$A=\frac{1}{\pi}\frac{\mu_0 r_h H_c}{g}\left[-2\sin\delta\left(\delta-\alpha+\sqrt{K^2-1}\right)-2\cos\delta-\frac{K}{2}\left(\cos 2\delta-\cos 2\alpha\right)+2K\right]$$

$$B=\frac{1}{\pi}\frac{\mu_0 r_h H_c}{g}\left[-\frac{\sqrt{K^2-1}}{K}-K\left(\delta-\alpha\right)+2\sin\delta+2\cos\delta\left(\frac{K\sin\delta}{2}-\delta+\alpha-\sqrt{K^2-1}\right)\right]$$

Therefore $J=\sqrt{A^2+B^2}$

$$\beta=\tan^{-1}(B/A)$$

2.3 EQUIVALENT CIRCUIT OF IDEALISED CIRCUMFERENTIAL-FLUX MACHINE

The flux linkage λ_a of phase a of the stator winding due to the air-gap flux may be determined by first finding the flux linkage of a single turn with sides θ and $\theta+\pi$.

$$\lambda_\theta = \int_\theta^{\theta+\pi} B_{g\theta} r_g l \, d\theta$$

$$= \frac{-2\mu_0 r_h H_c r_g l J}{g} \cos(\omega t - \theta - \beta) \quad \ldots \ldots (2.20)$$

+ higher odd harmonic terms, using equation (2.20) to define $B_{g\theta}$. The axial length of the rotor is l. The air-gap flux linkage of the complete stator winding of phase 'a' is then found to be, using equation (2.1):

$$\lambda_a = \int_\pi^0 \frac{N_s \sin\theta}{2} \lambda_\theta d\theta$$

$$= \frac{\pi}{2} \frac{N_s \mu_0 r_h H_c r_g l J}{g} \sin(\omega t - \beta) \text{ webers} \quad \ldots \ldots (2.21)$$

This flux linkage has no time harmonic terms. Following equations (7) and (27) Ref. (7), let the inductance corresponding to the air-gap reluctance be

$$L_g = \frac{\pi}{8} \frac{N_s^2 \mu_0 r_g l}{g} \text{ Henrys} \quad \ldots \ldots \ldots \ldots (2.22)$$

Let the effective value of current in phase 'a' be I_a. Then the effective value of the voltage induced in the stator winding of phase 'a' is

$$E_p = j\omega \frac{\lambda a}{\sqrt{2}} \quad \ldots\ldots\ldots\ldots\ldots\ldots (2.23)$$

Combining equations (2.21), (2.22) and (2.23) gives

$$E_p = \omega L_g \left(\frac{4 r_h H_c}{\sqrt{2} m N_s} \right) J \angle \frac{\pi}{2} - \beta \text{ Volts (rms).} \quad \ldots (2.24)$$

The similarity between this equation (2.24) and equation (39) of Ref. (7) demonstrates that this circumferential- flux machine can be represented by a simple electrical equivalent circuit of the form shown in Fig. (2.6).

Here the stator leakage inductance L_{ls} and the stator resistance R_s have been added to extend the circuit to the terminals of the machine.

2.4 IMPROVED MODEL FOR B—H LOOP

The equivalent circuit for circumferential-flux machine shown in Fig. (2.6) is simpler than that developed for the radial-flux machine in Fig. (10) of Ref. (7). The reason for this is that the B-H loop of Fig. (2.4) assumes infinite unsaturated permeability and zero saturated permeability for the hysteresis material. A better model for a practical B-H loop would be that of Fig. (2.7) in which the unsaturated relative permeability μ_{r0} is finite and the saturated relative permeability μ_{rs} is greater than unity.

The relationship between the flux densities in the air gap and in the hysteresis material is given in equation (2.11). Differentiating the eqn. (2.11) with respect to θ and combining the result with equation (2.5) gives

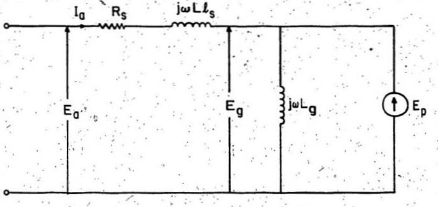

FIG. 2.6 EQUIVALENT CIRCUIT FOR CIRCUMFERENTIAL-FLUX MACHINE, BASED ON B-H LOOP OF FIG. 2.4

$$h\frac{d^2B'_{h\theta}}{d\theta^2} = r_g\frac{dB_{g\theta}}{d\theta}$$

$$= \frac{\mu_0 r_g r_h}{g} H'_{h\theta} - \frac{\mu_0 r_g}{g}\frac{mN_s\hat{I}}{4}\text{Cos }(\omega t-\theta) \quad \ldots\ldots\ldots (\ 2.25\ )$$

where the relationship between the circumferentially directed $B'_{h\theta}$ and $H'_{h\theta}$ is shown in **Fig.** (2.7). Following a procedure similar to that demonstrated in **Fig.** (4.) of **Ref.** [7], the relationship of B'_h and H'_h in Fig. (2.7) can be related to the B_h/H_h characteristic of **Fig.** (2.4) by the equations

$$H'_h = H_h + B'_h/\mu_{r0}\mu_0 \quad \text{amperes per meter} \quad (\ 2.26\ )$$

and

$$B'_h = B_h + \mu_p\mu_0 H_h \quad \text{webers per meter}^2 \quad (\ 2.27\ )$$

where

$$\mu_p = \frac{\mu_{rs}\mu_{r0}}{\mu_{r0} - \mu_{rs}} \quad \ldots\ldots\ldots\ldots (\ 2.28\ )$$

To conform with the analysis of the Ref. [7], let

$$\phi'_{h\theta} = hlB'_{h\theta} \text{ webers} \quad \ldots\ldots\ldots\ldots (\ 2.29\ )$$

and

$$\phi_{h\theta} = hlB_{h\theta} \text{ webers} \quad \ldots\ldots\ldots\ldots (\ 2.30\ )$$

Inserting equations (2.26), (2.27),(2.29) and (2.30) into equation (2.25) gives

$$R_g\frac{d^2\phi'_{h\theta}}{d\theta^2} = R_0\phi'_{h\theta} + R_p(\phi'_{h\theta} - \phi_{h\theta}) - \frac{mN_s\hat{I}}{4}\text{Cos }(\omega t-\theta) \quad \ldots\ldots (\ 2.31\ )$$

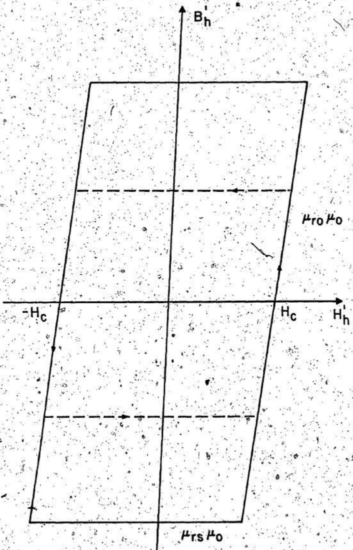

FIG. 2.7 IDEALIZED MAGNETIZATION CHARACTERISTIC WITH FINITE UNSATURATED PERMEABILITY AND SATURATED PERMEABILITY>1.0

where the air-gap reluctance R_g, the incremental unsaturated reluctance R_0, and the effective incremental saturated reluctance R_p of the hysteresis material per unit angle are given by

$$R_g = \frac{g}{\mu_0 r_g l} \quad \text{amperes per weber-radian} \quad \ldots \quad (2.32)$$

$$R_0 = \frac{r_h}{\mu_{r0}\mu_0 h l} \quad \text{amperes per weber-radian} \quad \ldots \quad (2.33)$$

$$R_p = \frac{r_h}{\mu_p \mu_0 h l} \quad \text{amperes per weber-radian} \quad \ldots \quad (2.34)$$

Equation (2.31) is of second order and is nonlinear. This may be represented by the equivalent magnetic circuit shown in the Fig. (2.8).

For specific value of the reluctances R_g, R_p and R_0 and for a given value of current $\hat{I}$, a set of solutionscan be obtained; but this set of solutions is too cumbersome to evaluate and plot for ranges of values of all parameters. By representing the element ($-R_g d^2\phi'_{h\theta}/d\theta^2$) of equation (2.31) by a simple reluctance, thus making equation (2.31) a linear algebraic one, a simple but approximate solution could be developed. If the distribution of flux $\phi'_{h\theta}$ with respect to θ is sufficiently close to sinusoidal in form, a double differentiation with respect to θ would cause a shift of a half period in the wave or a reversal of sign. The element then could be represented by the air-gap reluctance R_g, that is

$$-R_g \frac{d^2\phi_{h\theta}}{d\theta^2} \cong R_g\phi'_{h\theta} \quad \ldots\ldots\ldots\ldots \quad (2.35)$$

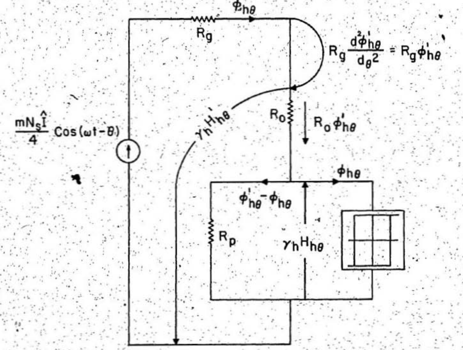

FIG. 2.8 EQUIVALENT MAGNETIC CIRCUIT FOR INCREMENTAL WEDGE OF CIRCUMFERENTIAL-FLUX MACHINE

This is a very big approximation. Then the equivalent circuit of Fig. (2.8) would contain only reluctance, a source mmf, and the ideal rectangular-loop hysteresis element. In this analysis, Thevenin's theorem is applied at the terminals of the ideal hysteresis element in Fig. (2.8) to represent the remainder of the circuit by a mmf (F_q) per unit angle, in series with a reluctance (R_q) per unit angle, where

$$F_q = \left(\frac{R_p}{R_p + R_0 + R_g}\right)\frac{mN_s\hat{I}}{4} \text{ Cos } (\omega t - \theta) \text{ amperes} \quad \ldots (2.36)$$

$$= r_h H_c K \text{ Cos } (\omega t - \theta)$$

$$R_q = \frac{R_p \ (R_0 + R_g)}{R_p + R_0 + R_g} \text{ amperes per weber-radian} \quad \ldots (2.37)$$

The resultant single-loop magnetic circuit is analysed in Ref. [7] and, after Fourier analysis, the fundamental component of flux per unit angle in the ideal rectangular-loop element is given by

$$\phi_{p\theta} = \frac{r_h H_c}{R_q} J \text{ Cos } (\omega t - \theta + \beta) \quad \ldots \ldots \ldots \ldots (2.38)$$

where factor J and angle β for this first approximate solution are plotted as a function of ratio K as defined in equation 2.36 in Fig. (2.9).

The dual electric equivalent circuit of Fig. (2.8) is shown in the Fig. (2.10), wherein the ideal hysteresis element is represented by the source voltage E_p

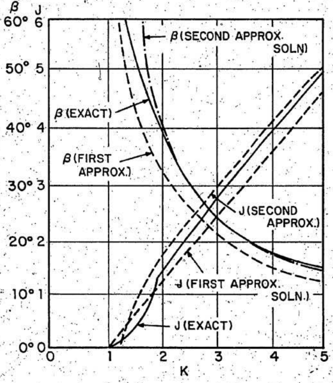

FIG. 2.9 COMPARISON OF FACTOR K AND ANGLE β FROM FIRST AND SECOND APPROXIMATE ANALYSIS OF FIG. 2.7 WITH THAT OBTAINED IN EXACT ANALYSIS OF LOOP OF FIG. 2.4

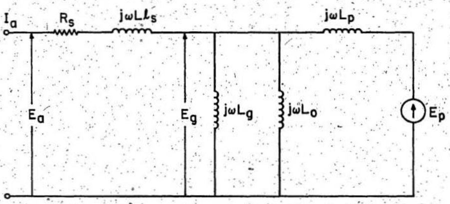

FIG. 2.10 EQUIVALENT CIRCUIT OF CIRCUMFERENTIAL FLUX MACHINE BASED ON B-H LOOP OF FIG. 2.7

where

$$E_p = \omega L_q \left(\frac{4r_h H_c}{\sqrt{2}mN_s}\right) J \underline{/\pi/2-\beta} \quad \text{volts (rms)} \; . \; . \; . \; (2.39)$$

$$L_q = \frac{m\pi N_s^2}{8R_q} \quad \text{henrys} \; . \; . \; . \; . \; . \; . \; . \; . \; . \; . \; . \; (2.40)$$

substituting the value of Rq from equation (2.37) in equation (2.40),

$$L_q = \frac{m\pi}{8} \; \frac{N_s^2 \; (R_p + R_0 + R_g)}{R_p \; (R_0 + R_g)} \quad \text{Henry} \; . \; . \; . \; . \; . \; (2.41)$$

the inductances in Fig. (2.10) are related to their corresponding reluctances in Fig. (2.8), by equation similar to (2.41).

Factors J and angle β for the exact first-approximation analyses should be identical when $\mu_{rs} = 0$, and $\mu_{r_0} = \infty$ in Fig. (2.7), leaving only the air-gap reluctance in Fig. (2.8). In Fig. (2.9), the approximate analysis gives values of J which are high for $K<K_c$ and low for $K>K_c$ while the values of β are low for all values of K. This approximate analysis is, however, close enough to be useful. For machines in which the air-gap reluctance is not the dominant element in the magnetic circuit of Fig. (2.8), this first approximate analysis should be quite accurate. For machines in which the air-gap reluctance is the dominant quantity, the exact analysis developed at the beginning of this chapter gives the best accuracy.

2.5 SECOND METHOD OF APPROXIMATE ANALYSIS

The values of K,J and β for the second approximate solution are shown in the Fig. (2.9), together with those of the first approximate solution and the exact solution for the simple B-H loop. The results of the second approximate solution are quite close to that of the exact solution for large values of K. With a high current in the stator giving a large value of K, the mmf drop in the reluctance, particularly the air gap, greatly exceeds that required for coercive force in the hysteresis material. Under this condition, the flux is expected to be nearly sinusoidally distributed in space and time, and the approximation on which the analysis is based is resonably accurate.

From another viewpoint, the exact solution showed that, for $K>1.862$, the rotor material spends all its time on the sides of the B-H loop, making an instantaneous jump across the top and bottom of the loop at the transition angles α and $\alpha+\pi$. Equations of type (2.8) then apply throughout the air gap. For large values of K, this solution approaches a sinusoid. From equation (2.11), the circumferential flux, being differentially related to the air-gap flux, will rapidly approach a sinusoid because of the large values of K.

2.6 TORQUE IN THE MACHINE

The torque of the machine is equal to the power crossing the airgap per unit of angular velocity of the rotating field.

Using the equation (2.36), (2.39) and (2.41), the torque for a 2-pole m-phase machine is

$$T = mL_q \left(\frac{4r_h H_c}{\sqrt{2} m N_s}\right)^2 JK \sin\beta \text{ Newton-meters} \quad \ldots (2.42)$$

The function JK sin β is plotted in Fig. (2.11) for (i) the exact analysis of the simple B-H loop model, (ii) the first approximate analysis.

The expression of the torque given by the equation (2.42) is however valid for parallelogram model neglecting the parasitic losses at synchronous mode. Detailed derivation of sub-synchronous phasor representation including both mmf and flux parasitic losses are given in Ref. [15]. Fig. (17) of Ref. [7] shows the predicted characteristic together with the measured curve of maximum torque near synchronism as a function of stator current. The rounding of the experimental curve is explained by the corresponding rounding of the B-H loop, particularly near the saturation.

In the analytical approach of developing the necessary equations to determine the motor terminal quantities such as voltage, current and power factor, the non-linear characteristic of B-H loop is simplified utilising the linear properties. The precise consideration of minor loops also becomes a difficult task. This gives rise to erroneous terminal quantities of the hysteresis motor. Also it is difficult to represent the B-H loop, maintaining all the basic qualities of it by any analytical means.

The torque produced in a hysteresis motor is proportional to the actual area of the hysteresis loop. Therefore, the best method to accomodate the the hysteresis loops taking into consideration

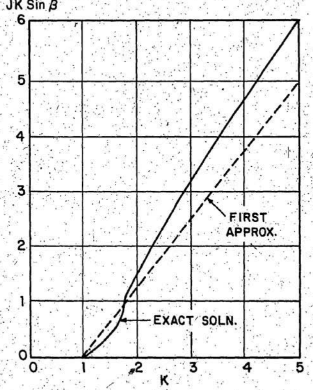

FIG. 2.11 TORQUE FUNCTION JK sin β FOR VARIOUS METHODS OF ANALYSIS

saturation is perhaps by modelling of B-H loop by discrete digital points. Hence the modelling of the B-H loop using digital techniques is the next best alternative.

CHAPTER III

MODELLING OF B-H LOOP

3.1 INTRODUCTION

It is a well known fact that the analysis of the hysteresis machine depends how we represent the actual B-H loop, keeping its basic properties similar to that of the original one. The analysis of a circuit having non-linear element is a difficult task. To represent the B-H loop and to find the motor dimensions, in terms of the properties of the rotor magnetic material, it is very essential to represent it in a suitable way. The analysis of the machine becomes impossible if one sticksto the actual B-H loop. Analyses of the motor behaviour have been made using ellipse and parallelogram to represent the hysteresis non-linearity. Copeland and Slemon [7, 8] use the field parallelogram approach, Robertson and Zaky [12] use the field ellipse approach, and O'Kelly [24] uses the circuit ellipse method. It is necessary to know the characteristic curves of the ring material and also to be able to represent them in some way.

Poritsky and Butler [26] consider the non-linear relationship of the B-H curve to find the mathematical interpretation. The firstattempt was made to represent a certain portion of the loop by an empirical formula, e.g., $B = B_s(1-e^{-a_1(H_s+H_c)})$. In addition, Gillot and Abrams [27], Bullingham, Bernol [28] Zakrazewski and Pietras [29] have also suggested the static B-H loop representation.

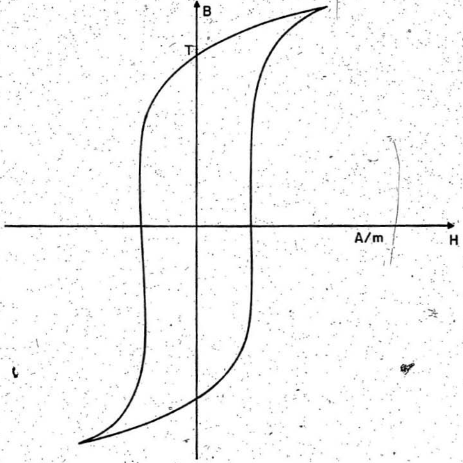

FIG. 3.1 CHARACTERISTIC CURVE OF HYSTERESIS RING MATERIAL

In addition, the suggestions given by Fisher and Moser [30], Davis [31], Trutt, Erdelyi and Hopkins [32] and Widger [33], are also of high importance in the static B-H loop representation.

The approximate theory for calculating the torque of the hysteresis motor was first developed by Teare [10]. In hysteresis machine, full representation of B-H loop is very essential. In the uniform rotating field, the B-H relationship for components is an inclined ellipse. Because of this, Teare assumed an elliptical model for the hysteresis loop. The equivalent ellipse is chosen so that the area and the maximum value of B are the same as those of the corresponding loop. Thus the hysteresis loop is replaced by an elliptical model in his analysis of the hysteresis motor. The elliptical representation was further extended by Roters [11], Miyairi [13] and Robertson [12] for the fractional hp synchronous hysteresis motor. O'Kelly [14] further extended the elliptical representation of hysteresis loop, and analysed the hysteresis motor accordingly by replacing the rotor material by closed coils.

In case of elliptical representation, the B-H loop is modified to an elliptical shape. By this method of representation, the higher remanent flux density which is required for the higher starting torque is possible. Thus, in this method the area of the hysteresis loop is almost replaced by the same area as that of the B- H loop. The area of the loop, can easily be found which is proportional to the torque produced in the rotor material. Presiach-Neel's model has been used by J.Peard and M.Polojadoff in the study of the 'performance of hysteresis motor'. This model seems to work very well for particular type of hysteresis material. However, it is found that the Frölich approach gives a better B-H loop for most of the hysteresis materials.

3.2 BASIC ELLIPTICAL MODEL

Considering the concept of complex permeability the B-H relation can be defined as $B = \mu_r e^{-j\theta}$, where θ is known as the hysteresis angle. If the magnetising field is $H_s \sin \omega t$, then $B = \mu_r H_s \sin(\omega t - \theta)$. Eliminating the sinusoidal time function the equation of the elliptical hysteresis is

$$\frac{H}{(H_s \sin\theta)^2} + \frac{B}{(\mu_r H_s \sin\theta)^2} - \frac{2BH\cos\theta}{\mu_r (H_s \sin\theta)^2} = 1 \quad \ldots (3.1)$$

The semi-major axis, semi-minor axis and the angle τ shown in the Fig. (3.2) are approximately $\mu_r H_s$, $H_s \sin\theta$ and $\cos\theta/\mu_r$ respectively. Therefore the area of the loop is $\pi\mu_r H_s^2 \sin\theta$, where μ_r is determined from the static B-H loop as follows:

$$\mu_r = \frac{B_s}{H_s} \quad \ldots\ldots\ldots\ldots\ldots\ldots (3.2)$$

The hysteresis angle is obtained by equating the area of static B-H loop to that of the area of the ellipse

$\pi\mu_r H_s^2 \sin\theta$ = Area of the actual loop. Taking into consideration the elliptical approximations, the complex permeability [34, 24] of the rotor hysteresis material is given by $\mu = \mu_r e^{j\beta}$, such that the magnetic field intensity H is written as

$$H = \mathrm{Re}\{\hat{H} e^{-j\omega t}\} \quad \ldots\ldots\ldots\ldots\ldots (3.3)$$

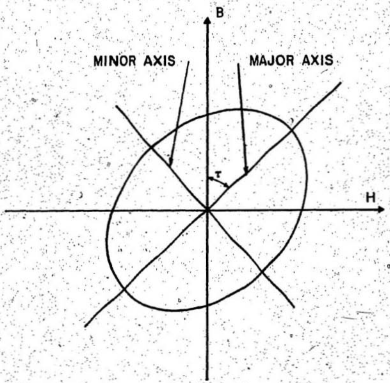

FIG. 3.2 ELLIPTICAL REPRESENTATION OF B-H LOOP

The corresponding magnetic flux density B is given as

$$B = R_e \{ \hat{B} e^{-j(\omega t - \beta)} \} \quad \ldots\ldots\ldots\ldots (3.4)$$

The rotor hysteresis material's relative permeability μ_r and hysteresis lag angle β can be easily obtained from the given hysteresis loop of the material.

3.3 FRÖLICH'S MODEL

In Fig. (3.3) the major B-H loop is essentially divided into four portions and each portion is represented by Frölich's curve, with centers are at c and f ($H = \pm H_c, B=0$). The abcd portion of the loop as shown in Fig. (3.3) is opposite in sign to that of defa. Therefore, if the upper portion of the loop can be represented by some formula, then lower portion can be found automatically. The portion gbc is represented as follows,

$$B_{gbc} = \frac{H + H_{cc}}{E + F (H + H_{cc})} \quad \ldots\ldots\ldots (3.5)$$

A Frölich curve is used in order to obtain the actual curve i.e., abc,

$$B_{abc} = \frac{(H + H_{cc})}{E + F (H + H_{cc})} + GH \quad \ldots\ldots (3.6)$$

If $H < 0$, then $G = 0$.

The portion of the loop cd is represented by

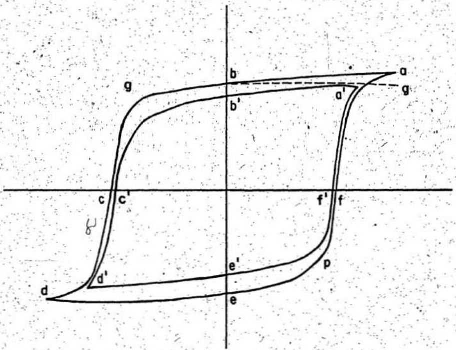

FIG. 3.3 STATIC B-H LOOP

$$B_{cd} = \frac{(H + H_c)}{EE - EF\,(H + H_c)} \quad \ldots\ldots\ldots\ldots (3.7)$$

Similarly,

$$B_{def} = \frac{(H - H_{cc})}{E - F\,(H - H_{cc})} + GH \quad \ldots\ldots\ldots (3.8)$$

and

$$B'_{fa} = \frac{(H - H_c)}{EE + FE(H - H_c)} \quad \ldots\ldots\ldots\ldots (3.9)$$

In the above equations (3.5 – 3.9), the values of E, F, EE, FF, are all constants, and they are obtained by plotting the reciprocals of B and H, which give a straight line. The slope of the line is E or EE and the intercept of the line on the Y-axis is F or FF, depending on the portion of the loop.

The equation of the straight line representing gbc portion of the curve is,

$$\frac{1}{B} = \frac{E}{H} + F \quad \ldots\ldots\ldots\ldots\ldots\ldots\ldots (3.10)$$

Similarly for the portion cd it is

$$\frac{1}{B} = \frac{EE}{H} + FF \quad \ldots\ldots\ldots\ldots\ldots\ldots\ldots (3.11)$$

The B-H relationship in the material is no longer described by the B-H loop for the surface, when the amplitude of the applied magnetic field begins to decrease within the material. But it is described by one of the minor loops of Fig. (3.3).

The method by which any of these is determined, using the known data describing the major saturated hysteresis loop is described as below.

The portion dc of the major loop fits well with the similar portion of the minor loop by changing the centre ($H = H_c$, $B = 0$). That is by changing the value of coercive force (H_c) of the major B-H loop to the value of the coercive force corresponding to the minor loop.

Equations (3.6) and (3.7) are modified as follws, in order to calculate the value of flux density (B) for the minor loops,

$$B_{abc} = \frac{(H + H_{cc})}{E + F\ (H + H_{cc})} + GH - (B_{r}max - B_r) \quad (3.12)$$

if $H<0$, $G = 0$

$$B_{cd} = \frac{(H + H_c)}{EE - EF\ (H + H_c)} \quad (3.13)$$

Similarly equations (3.8) and (3.9) are changed to

$$B_{def} = \frac{(H - H_{cc})}{E - F\ (H - H_{cc})} + GH + (B_{r}max - B_r) \quad (3.14)$$

if $H > 0$, then $G = 0$

$$B_{fa} = \frac{(H - H_c)}{EE + EF\ (H - H_c)} \quad (3.15)$$

The H_{cc} and $B_{r}max$ are the values of coercive force and residual magnetisation respectively of the loop from which the values of flux density are calculated for the loop nested within it.

3.4 PARALLELGRAM MODEL

Copeland and Slemon introduced the parallelogram model in the analysis of hysteresis motor. They predicted the fundamental developed torque in terms of machine dimensions and hysteresis material characteristics, namely the permeabilities and hysteresis lag angle. The parallelogram modelling has been carried out, considering the width of it is equal to twice the coercive force of the material. It is however, claimed that the rotor reactance is represented in a better way, compared to elliptical model.

In the hysteresis material the magnetic flux per unit angle ϕ_θ is related to the magnetic potential $F_{h\theta}$ across the material by the idealized characteristic of Fig. (3.5). This is derived from the B–H characteristic of the rotor hysteresis material Fig. (3.4) and is linearly related to it by

$$\frac{\phi_\theta}{B_h} = r_h l \quad \text{meters}^2 \quad \ldots\ldots\ldots\ldots (3.16)$$

and

$$\frac{F_{h\theta}}{H_h} = h \quad \text{meters} \quad \ldots\ldots\ldots\ldots\ldots (3.17)$$

Any flux excursion on the Fig. (3.5) is governed by a straight- line relation of the y = mx + c, where $\frac{1}{R_a}$ is the slope if the state-point is on the left or right hand side of the loop, and $\frac{1}{R_s}$ if the state-point is within the outer boundaries of the loop. These incremental reluctances per unit angle are given by expressions

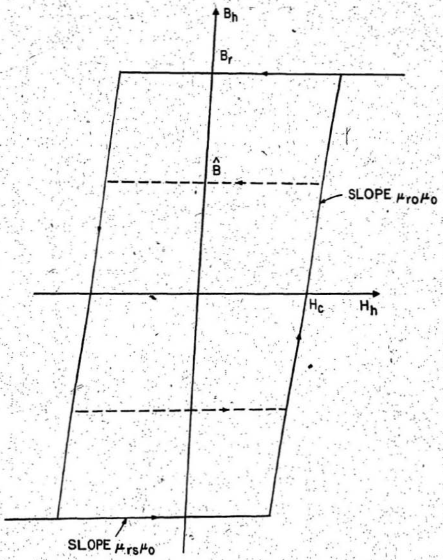

FIG. 3.4 IDEALIZED MAGNETIZATION CHARACTERISTIC FOR HYSTERESIS MATERIAL

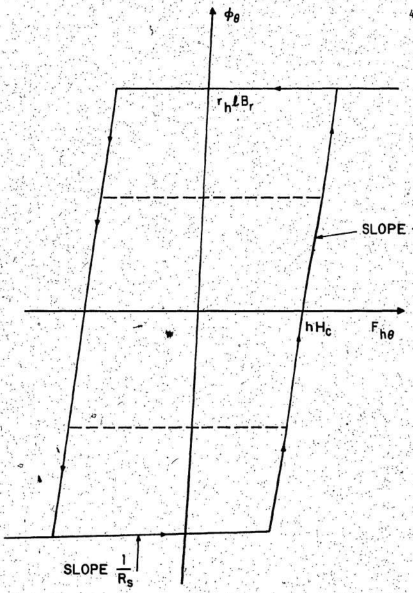

FIG. 3.5 FLUX PER UNIT ANGLE VS MAGNETIC POTENTIAL FOR HYSTERESIS MATERIAL IN MACHINE

$$R_0 = h/\mu_{r0}\mu_0 r_h l \quad \text{amperes per weber radian.} \ldots (3.18)$$

$$R_s = h/\mu_{rs}\mu_0 r_h l \quad \text{amperes per weber radian.} \ldots (3.19)$$

This characteristic may be represented as a linear reluctance per unit angle R_0 in series with a vertically sided ϕ/F characteristic as shown in Fig. (3.6a) and (3.6b). The linear reluctance R_0 of Fig. (3.6a) has an effect which is equivalent to an extension of the air gap. The new loop has vertical sides,i.e., zero reluctance. Because of the subtraction of $\frac{1}{R_0}$ everywhere from the slope of the loop, any flux excursion within the outer boundaries of the new loop will occur with a slope $\frac{1}{R_p}$ where

$$R_p = R_s - R_0 \quad \text{ampere per weber radian} \ldots (3.20)$$

The nonlinear characteristic of Fig. (3.6b) can be further simplified by representing it as a linear reluctance per unit angle R_p in parallel with a rectangular loop nonlinear element as shown in Fig. (3.6c) and (3.6d).

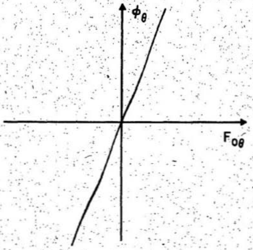

FIG. 3.6a RELUCTANCE PER UNIT ANGLE R_θ

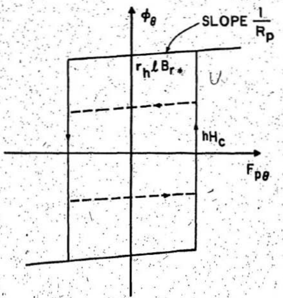

FIG. 3.6b ORIGINAL CHARACTERISTIC OF FIG. 3.5 WITH SERIES RELUCTANCE R_θ' SUBTRACTED

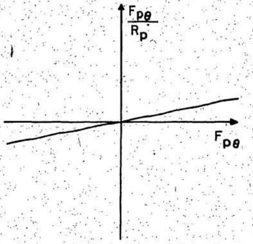

FIG. 3.6c RELUCTANCE PER UNIT ANGLE R_p

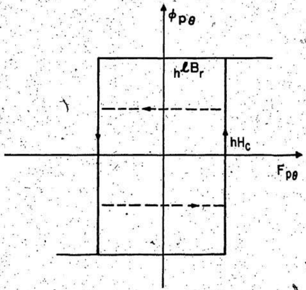

FIG. 3.6d CHARACTERISTIC OF FIG, 3.6b WITH PARALLEL RELUCTANCE R_p SUBTRACTED

CHAPTER IV

DIGITAL SIMULATION OF B-H LOOP

4.1 INTRODUCTION

In the preceding chapter different ways of graphical and analytical representation of B-H loops have been introduced. Consideration of idealised B-H characteristics enables the desirable properties or ' goodness' of the rotor material of a hysteresis machine to be assessed. Type of B-H loop approximations to be made depends upon the magnetic properties of the rotor magnetic materials.

It has been learnt from the fundamental principle of hysteresis machine, that the torque produced is directly proportional to the area of the B-H Loop of the rotor magnetic material. Thus the entire performance of the machine depends primarily on the optimized representation of the actual B-H loop of the material.

A number of attempts were made by several Investigators [22, 35, 36, 37] to develop a computer programme in order to simulate B-H loop of non-linear elements. In 1970, J.S. Everatt developed an algorithm to simulate the B-H loop of any non-linear element based on the modified Frölich's approach, given in the next section.

The digital simulation of hysteresis loop plays a major role, in predicting the behaviour of hysteresis motor by the use of modern digital computers available, in terms of machine dimensions, winding data, and in terms of the properties of the rotor magnetic material.

4.2 MODIFIED FRÖLICH'S MODEL

By using the more successful mathematical representation derived from Lamont's law, which states that the permeability of the magnetic material is proportional to its degree of magnetisation.

$$\mu = K(B_s - B) \quad \ldots\ldots\ldots (4.1)$$

where K is a constant

Since $\mu = \frac{B}{H}$

$$\frac{B}{H} = KB_s - KB \quad \ldots\ldots\ldots (4.2)$$

$$B = \frac{KHB_s}{1 + KH} = \frac{H}{b + cH} \quad \ldots\ldots\ldots (4.3)$$

where b and c are constants, c being $1/B_s$.

In applying these relations to the permanent magnet demagnetisation curve it is necessary to displace the curve by the amount of coercive force (Hc). The equation for a demagnetisation curve then becomes:

$$B = \frac{H + H_c}{b + C(H + H_c)} \quad \ldots\ldots\ldots (4.4)$$

when $H = 0$, $B = B_r$,

and $B_r = \frac{H_c}{b + CH_c}$ $\quad \ldots\ldots\ldots (4.5)$

$$b = \frac{H_c}{B_r} - \frac{H_c}{B_s} \quad \ldots\ldots\ldots (4.6)$$

or since $C = \frac{1}{B_s}$

$$B = \frac{H + H_c}{(H_c/B_r) + (H/B_s)} \quad \ldots\ldots\ldots\ldots\ldots\ldots (4.7)$$

To find the value of B_m which makes BH a maximum, the above expression is multiplied by H and differentiated and equated to zero.

$$BH = \frac{H^2 + HH_c}{b + c(H + H_c)} \quad \ldots\ldots\ldots\ldots\ldots\ldots (4.8)$$

$$\frac{d(BH)}{dH} = \frac{[b + c(H + H_c)]\ [(2H + H_c) - (H^2 + H_cH)c]}{[b + c(H + H_c)]^2} = 0 \quad \ldots (4.9)$$

solving this expression yields the following expressions for B_m and H_m:

$$B_m = (1/c)(\sqrt{1 - cB_r} - 1) \quad \ldots\ldots\ldots\ldots (4.10)$$

$$H_m = (H_c/cB_r)\ (\sqrt{1 - cB_r} - 1) \quad \ldots\ldots\ldots\ldots (4.11)$$

In a similar way the expressions for the remaining quadrants of the loop can be developed. Thus the simulation of the complete hysteresis loop is made by analytical expressions.

Everatt developed a numerical method utilising the modified Frolich curve, which made the computer simulation of non-linear hysteresis loop possible for specific application. This technique is utilised to simulate the entire B-H loop for hysteresis motor application. The entire programming is based on the Everatt's method.

4.3 ALGORITHM

The magnetisation curve of the hysteresis material can be represented by [35],

$$B^* = \frac{aB_s H^*}{1 + bH^*} + \mu_0 H^* \quad \ldots \ldots \ldots \ldots \ldots (4.12)$$

which is a modification of the Frölich curve. Where $H^* \geq 0$

B^* = Flux density

B_s = saturation flux density

H^* = magnetic field intensity

a and B_s are constants which are determined from the actual magnetisation curve. The constant b is under the control of the algorithm and is initially equal to a. The hysteresis loop is constructed from four adjoining curve- segments, is shown in Fig. (4.1). Table (4.1) contains the values of B_m and H_m, which are the values of B and H at the last tip of the loop encountered. H_c is a function of B_m and H_{cmax}. In the beginning H_c is zero and is recalculated at each tip, according to the rules:

$$H_c = H_{cmax} \frac{|B_m|}{B_s} \quad \text{where } |B_m| \leq B_s \quad \ldots \ldots \ldots (4.13)$$

$$H_c = H_{cmax} \quad \text{where } |B_m| > B_s \quad \ldots \ldots \ldots \ldots (4.14)$$

Table (4.1) clearly shows that, the constants a and b are equal on segments 1 and 3. But the values of a and b are recalculated at each entry to segments 2 or 4.

4.4 SIMULATION EXAMPLES

The algorithm developed for modified Frölich approach given in earlier section is utilised in this section. This method

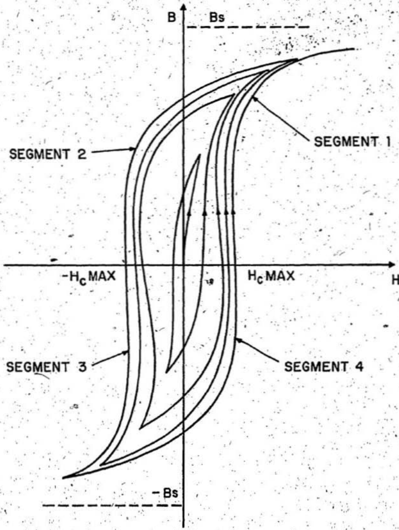

FIG. 4.1 GROWTH OF SIMULATED B-H LOOP

Table 4.1. Definitions of the Four Segments and Appropriate Changes of Variables.

	Segment 1	Segment 2	Segment 3	Segment 4
	$B > 0$, H increasing	$B > 0$, H decreasing	$B < 0$, H decreasing	$B < 0$, H increasing
B^*	$B^* = B$	$B^* = B$	$B^* = -B$	$B^* = -B$
H^*	$H^* = H - H_c$	$H^* = H + H_c$	$H^* = -H - H_c$	$H^* = -H + H_c$
b	$b = a$	$b = \frac{aB_s}{\lvert B_m\rvert - \mu_0(\lvert H_m\rvert + H_c)} - \frac{1}{\lvert H_m\rvert + H_c}$	$b = a$	$b = \frac{aB_s}{\lvert B_m\rvert - \mu_0(\lvert H_m\rvert + H_c)} - \frac{1}{\lvert H_m\rvert + H_c}$

have been tested in simulating 17% cobalt steel, 36% cobalt steel and oerstit-70 alloys.

Table (4.2) contains the pertinent magnetic properties of 17% cobalt steel, 36% cobalt steel and oerstit-70. However, it is known that Hc, Br, Bsat, and Hs of the hysteresis material vary to some extent depending upon its past history. The parameters of the respective hysteresis material given in Table (4.2) are inserted into the computer programme. The values of Hc and H_{cmax} are set within the reasonable value. It should be noted that the intersection on the H axis increases with decreasing ratio of Br/Hc.

The actual B-H loop of 17% cobalt steel, 36% cobalt steel, and Oerstit - 70 alloys are shown in Fig. (4.2), (4.3), and (4.4) respectively. The simulated B-H loop of 17% cobalt steel, 36% cobalt steel , and oerstit-70 are shown in Fig. (4.5), (4.6) and (4.7) respectively. Comparison between the simulated B-H loop and the actual B-H loop shows a very close agreement in all respect.

4.5 EFFECT OF HYSTERESIS PARAMETERS ON AIR-GAP POWER OF THE HYSTERESIS MACHINE

Fig. (4.8) shows the plot of air-gap power vs the unsaturated relative permeability. Fig. (4.9) shows the relation between the air-gap power and Br, which indicates that there is an enormous increase in air-gap power as the Br increases. The plot shown in Fig. (4.10) clearly reflects that there is a very less change in the air-gap power, as the saturated relative permeability is varied. The

Table 4.2 Pertinent Magneto-Electric properties of Hysteresis Materials.

	17% Cobalt Steel	Oerstit-70	36% Cobalt Steel
B_r	0.95 T	0.85 T	0.90 T
B_s	1.50 T	1.20 T	1.45 T
H_c	12.80 kA/m	12.50 kA/m	19.85 kA/m
μ_{rs}	14.60	14.90	12.00
H_s	28 kA/m	25 kA/m	34 kA/m

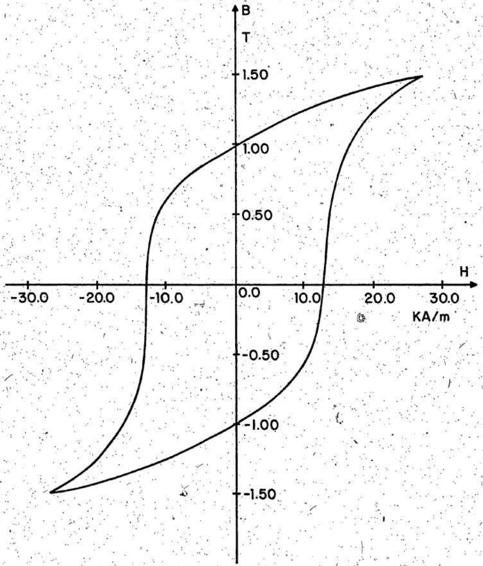

FIG. 4.2 B-H LOOP FOR 17% COBALT STEEL (ACTUAL)

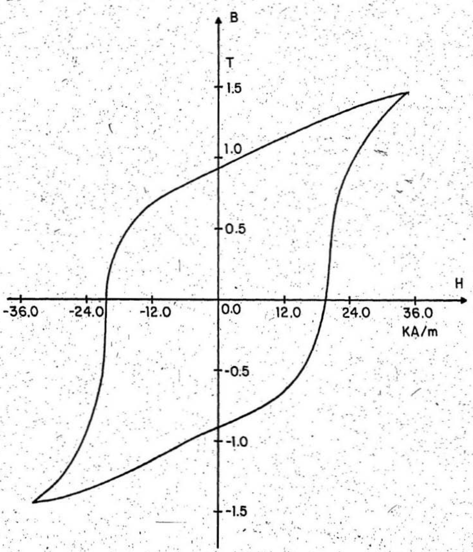

FIG. 4.3 B-H LOOP FOR 36% COBALT STEEL (ACTUAL)

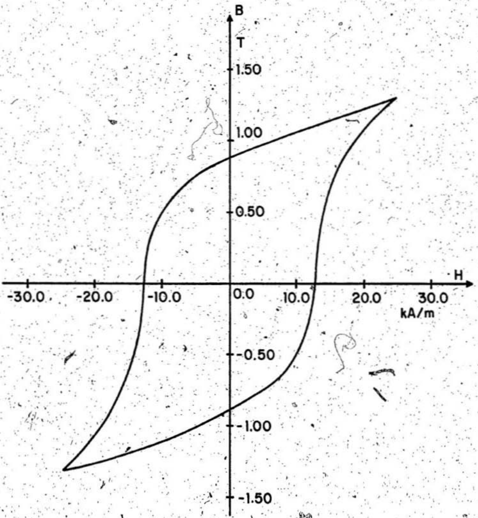

FIG. 4.4 B-H LOOP FOR OERSTIT-70 (ACTUAL)

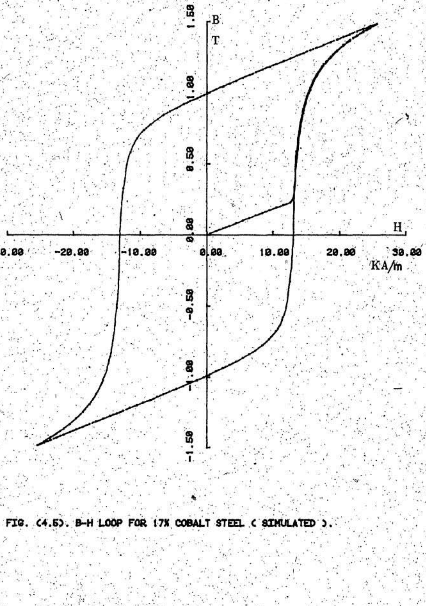

FIG. (4.5). B-H LOOP FOR 17% COBALT STEEL (SIMULATED).

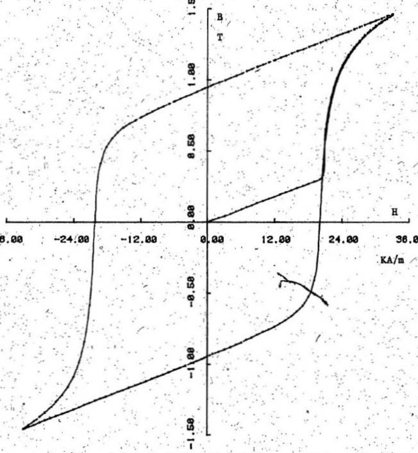

FIG. (4.8). B-H LOOP FOR 38% COBALT STEEL (SIMULATED).

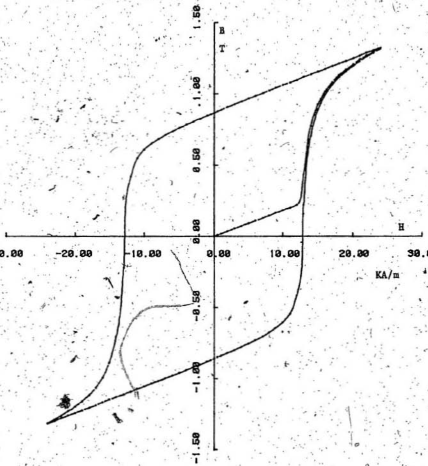

FIG.(4.7). B-H LOOP FOR OERSTIT-70 (SIMULATED).

PLOT AIR-GAP POWER VS UNSATURATED RELATIVE PERMEABILITY,
KEPPING THE FOLLOWING CONSTANT

(1). REMANENT FLUX DENSITY
(2). COERCIVE FORCE
(3). SATURATED RELATIVE PERMEABILIT

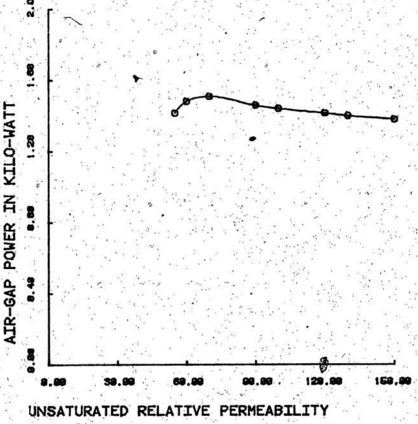

FIG. (4.8). AIR-GAP POWER VS UNSATURATED RELATIVE PERMEABILITY

PLOT AIR-GAP POWER VS REMANENT FLUX DENSITY:
KEEPING THE FOLLOWING CONSTANT
(1). UNSATURATED RELATIVE PERMEABILITY
(2). SATURATED RELATIVE PERMEAB
(3). COERCIVE FORCE

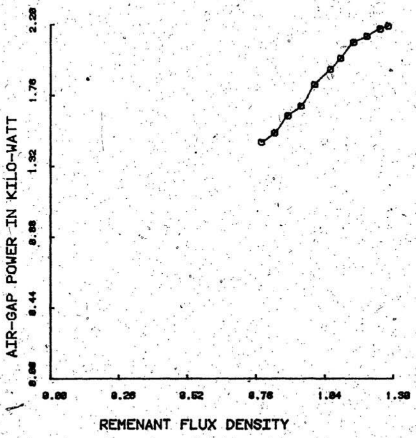

FIG. (4.9). AIR-GAP POWER VS REMANENT FLUX DENSITY

PLOT AIR-GAP POWER VS SATURATED RELATIVE PERMEABILITY,
KEEPING THE FOLLOWING CONSTANT
(1). UNSATURATED RELATIVE PERMEABILIT
(2). REMANENT FLUX DENSITY
(3). COERCIVE FORCE

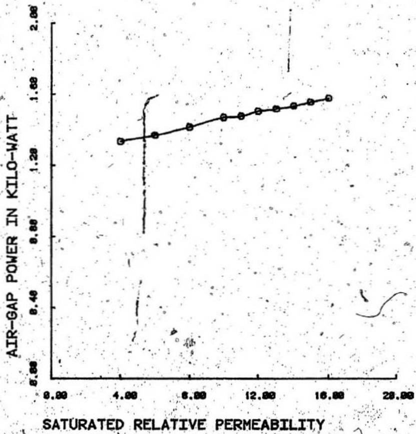

FIG. (4.10). AIR-GAP POWER VS SATURATED RELATIVE PERMEABILITY plot of air-gap power vs coercive force shown in Fig. (4.11), clearly indicates that there is a sudden rise in air-gap power up to certain value of the coercive force (about 13 kA/M),and decrease in power beyond this value of H_c.

PLOT AIR-GAP POWER VS COERCIVE FORCE:
KEEPING THE FOLLOWING CONSTANT
(1). UNSATURATED RELATIVE PERMEABILIT
(2). SATURATED RELATIVE PERMEABILITY
(3). REMANENT FLUX DENSITY

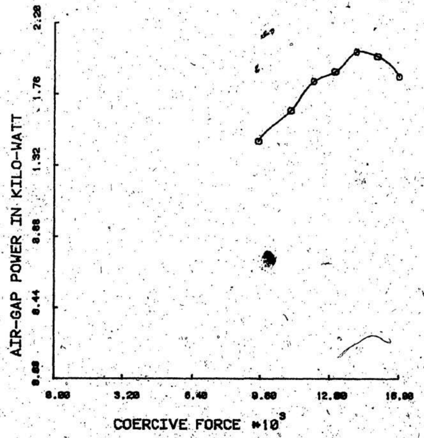

FIG. (4.11). AIR-GAP POWER VS COERCIVE FORCE

CHAPTER V

DIGITAL SIMULATION OF THE HYSTERESIS MOTOR

5.1 INTRODUCTION

The equations developed [8] to study the behaviour of the hysteresis motor is the landmark in the evolution of the hysteresis motor. These equations are developed by modelling the properties of rotor material with the help of idealised parallelogram of B-H loop. However, the equations developed to predict the torque of the idealised machine was exclusive off the parasitic losses associated with the rotor magnetic material, which is due to the excursion of the minor loop caused by the eddy current effect and tooth ripple present in the air-gap flux density.

5.2 EQUATIONS OF MOTOR

The equations used are based on those developed by Copeland and Slemon [8] for circumferential flux motor. The cross section of the circumferential-flux motor is as shown in the Fig. (5.1) It is important to note that the rotor core of the circumferential-flux is non-magnetic. The flux crosses the airgap radially and follows the circumferential path in the hysteresis ring.

The fundamental motor field equations for an m-phase, p-pole machine are given as:

$$\frac{g}{\mu_0}\frac{dB_{g\theta}}{d\theta} = H_{h\theta} r_h a - \frac{m}{2} N_s \hat{I}_a \left(\frac{2}{p}\right) \text{Cos}\left(\omega t - \frac{p\theta}{2}\right) \quad \ldots\ldots (5.1)$$

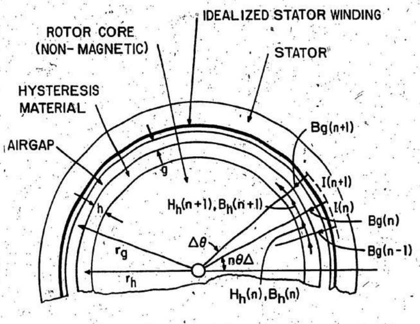

FIG. 5.1 CROSS-SECTION OF CIRCUMFERENTIAL FLUX HYSTERESIS MOTOR SHOWING DIMENSIONS AND ELEMENTAL SEGMENTS

$$h \frac{dB_{h\theta}}{d\theta} = r_g B_{g\theta} \quad \ldots\ldots\ldots\ldots\ldots (5.2)$$

According to the notation shown in the section of the motor Fig. (5.1), the following equations are developed for nth of $N = 2\pi/\Delta\theta$ segments [22] :

$$I(n) = r_h \Delta\theta H_h(n) + \frac{gh}{\mu_0 r_g \Delta\theta}\left[2B_h(n) - B_h(n-1) - B_h(n+1)\right] \quad (5.3)$$

$$B_h(n) = f[H_h(n)] \quad \ldots\ldots\ldots\ldots\ldots\ldots (5.4)$$

$$B_g(n) = \frac{h}{2r_g\Delta\theta}\left[B_h(n+1) - B_h(n-1)\right] \quad \ldots (5.5)$$

Equations (5.3) and (5.4) are solved for given stator mmf distribution $I(n,T)$, $n = 1, 2, \ldots\ldots\ldots N$. By knowing the previous state of the rotor at $T - \Delta T$, the magnetic state of the rotor of the idealised motor at time T is calculated. Equation (5.5) then gives the air gap flux, and from this the flux linkage per phase is computed knowing the stator winding distribution. The value of the stator induced voltage is then computed, and hence the motor shaft torque, by omitting windage and friction loss is carried out.

In the present study, provision is made to insert the stator winding resistance and leakage inductance in the above equations, and the corresponding changes are made in the computer programme to obtain the stator terminal voltage.

5.3 COMPUTER MODEL OF THE HYSTERESIS LOOP

The digital technique used in modelling the hysteresis loop is based on the piecewise linear approximations [22]. The model developed has got close association with the behaviour of many other permanent magnet materials which have got the required properties as rotors of the hysteresis motors.

The above mentioned model is found useful in solving the full motor equations by iteration method, which is a necessary factor for this type of problem. The magnetic flux density is defined by $y(T)$ and the magnetic field strength is defined by $x(T)$. T refers to time.

Thus the magnetic state of the material can be defined at any instant of time. The previous state of the material at any time is given by $(T-\Delta T)$. The previous state requires the three 'history' parameters $b(T-\Delta T)$, $c(T-\Delta T)$ and $m(T-\Delta T)$, apart from the values $x(T-\Delta T)$ and $y(T-\Delta T)$.

The allowable values of x and y are bounded in parallelogram set by H_c, B_r, α, β, and the tail representing the saturation Fig. (5.2a). In general, changes within this boundary follow lines with a slope α equal to that of the top of the parallelogram. Each point (x,y), however, has a horizontal recoil line associated with it, of length equal to or less than 2ρ, bounded by the points (b,y) and (c,y). For large changes in x, the horizontal line is dragged along by one of its ends. When x changes in direction, there is a horizontal movement to the other end of the line, and it is then dragged in the opposite direction. There are nine possible modes of operation ($-4 \leq m \leq 4$; m integer).

The length of the recoil line in each mode is given in table (5.1)

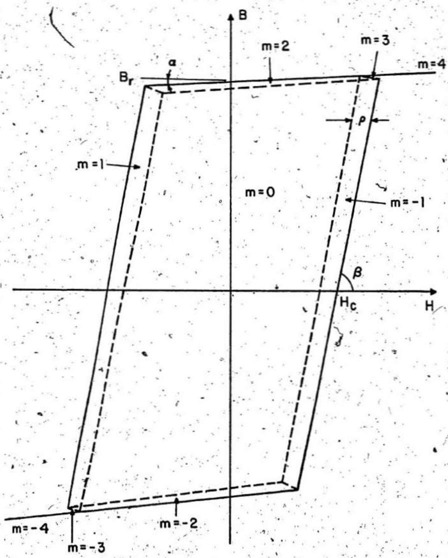

FIG. 5.2a LOOP PARAMETERS

Table 5.1 Length of recoil line

Mode m	Length of recoil line
0	$\rho < (c - b) < 2\rho$
$-2, -1, 1, 2$	ρ
$-3, 3$	$0 < (c - b) < \rho$
$-4, 4$	0

The possible B/H path is shown in the Fig. (5.2b). The 'history' parameters at each turning point of H are given in table (5.2).

Table 5.2 Co-ordinates of history parameters

Point	0	L	P	M	N
H	0	x_3	x_2	x_4	x_1
B	0	y_3	y_2	y_4	x_1
b	$-\rho$	$x_3 - \rho$	x_2	x_4	x_1
c	$+\rho$	x_3	$x_2 + 2\rho$	x_4	$x_1 + \rho$
m	0	-1	0	4	1

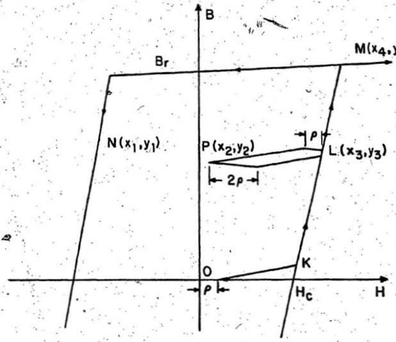

FIG. 5,2b POSSIBLE B/H PATH AS H IS VARIED

The subroutine employed in this case has to perform a long series of tests to establish new mode. To determine the new value of y, b and c at each mode, a function routine is employed. However, it does not require nonlinear function storage.

In the computer programme, 360 electrical degrees are divided into 36 segments. Idealised mmf distributions, corresponding to 18 and 3 slots per pole is used and the equations are solved for 180 electrical degrees only. An error function is used based on the successive approximations, which is reduced to a small value. The error function is of the form:

$$\epsilon(n) = I(n) - F[H_h(n), B_h(n), B_h(n-1), B_h(n+1)]. \quad (5.6)$$

The flow diagram for motor-equation program is shown in the Appendix E.

CHAPTER VI

RESULTS AND DISCUSSION

6.1 INTRODUCTION

In this chapter an attempt is made to study the performance characteristics of the hysteresis motor experimentally and to compare it with the computed results using the digital simulation method. The rotor hysteresis material used is made of 17% cobalt steel, supplied by the Permanent Magnet Manufacturing Company.

6.2 RING SPECIFICATION

Before going to study the performance of the hysteresis motor, it is essential to know the characteristic curve of the ring material and also to represent it in the form of B-H loop.

The heat treatment and annealing of the 17% cobalt steel was carried out at the Permanent Magnet Manufacturing Company. But the company could not provide the final B-H loop of the hysteresis ring material supplied. However, on testing the ring in the motor assembly, it was found that the sample ring did not give rise to the same values of B and H as specified for 17% cobalt steel material. However, on the basis of experimentat results the expected B-H loop of the sample ring was simulated and at values of $B_r = 0.80$ T, $\mu_{rs} = 10.00$, $\mu_{r0} = 100.00$ and $H_c = 9500.00$ A/m, the computer results and experimental results agrees within the limit of tolerance.

6.3 EXPERIMENTAL SETUP AND MEASUREMENT

Details of the experimental setupare given in the Appendix B. Two digital wattmeters were used to measure the input power to the machine. The design data of the hysteresis machine is given in the Appendix C.

The hysteresis motor was loaded by means of a d.c. work machine mechanically coupled with the experimental Mawdsleys Generalised machine. The machine was slowly loaded to the point of pull-out by varying the load resistance connected to the work machine.

The total input power less the total copper loss gives the air gap power. The output of the hysteresis machine is then calculated. The air-gap power less the rotor parasitic loss and friction and windage and core-loss gives the shaft output power. The parasitic loss was measured experimentally.

6.4 RESULTS

The efficiency and the full load input power factor of the hysteresis machine were calculated by knowing the output power and from the known values of terminal voltages and currents. Comparison of the experimental results and computed results show, a very close agreement. Tables (6.1) and (6.2) shows experimental results and computed results respectively.

The agreement between computed and measured results of Figs. (6.1) and (6.2) is reasonably good in view of the complexity

Table 6.1 Performance Results (Measured)

Current I_p (A)	Pull-in Voltage V_{L-L}	Power Factor	Air-gap Power (Watts)	Efficiency (%)
9.18	178.5	0.36	1077.50	58.0
9.84	190.0	0.37	1107.50	58.3
10.28	198.0	0.34	1184.00	60.0
10.82	205.0	0.33	1218.20	59.0
10.86	206.0	0.33	1235.70	56.50
10.94	208.0	0.33	1230.20	59.0

Table 6.2 Performance Results (Computed)

Current I_p (A)	Pull-in Voltage V_{L-L}(Volt)	Power Factor	Air-gap Power (Watts)	Efficiency (%)
9.18	190.0	0.41	998.0	73.0
9.84	199.0	0.39	1277.0	72.0
10.28	204.0	0.39	1261.0	71.0
10.82	210.0	0.34	1275.0	69.0
10.86	210.7	0.34	1270.0	69.5
10.94	212.0	0.34	1274.0	69.0

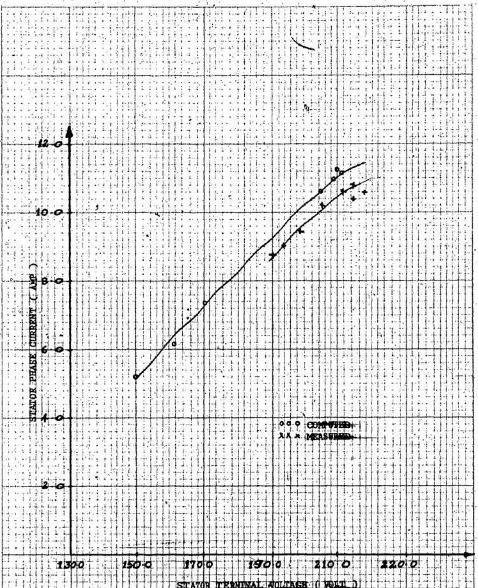

FIG. (6.1) MEASURED AND COMPUTED VALUES OF STATOR TERMINAL VOLTAGE AND PHASE CURRENT

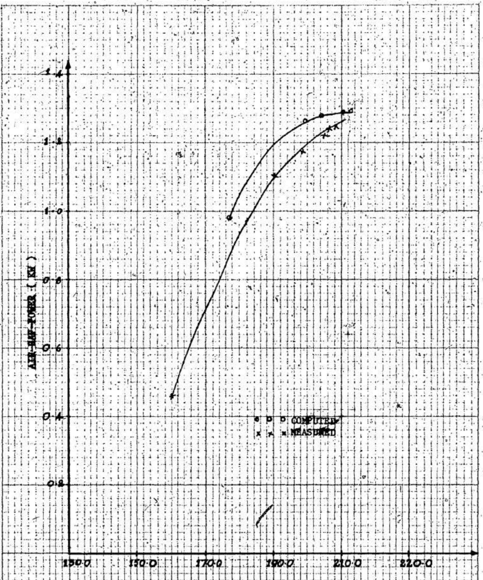

FIG. (6.2) MEASURED AND COMPUTED VALUES OF STATOR TERMINAL VOLTAGE AND AIR-GAP-POWER of the non-linearity of the hysteresis material and approximations made in the analysis. Fig. (6.1) shows the plot of terminal voltage vs stator phase current. Fig. (6.2) shows the plot of terminal voltage vs airgap power.

CHAPTER VII

CONCLUSIONS

Type of B-H loop approximations to be made depends upon the magnetic properties of the material. The performance of the hysteresis machine primarily depends upon the optimized representation of the actual B-H loop of the material, as it is used in predicting the terminal performances of the hysteresis motor. The digital technique based on the modified Frölich's approach is used in the simulation of the typical hysteresis materials like 17% cobalt steel, 36% cobalt steel and Oerstit-70 alloys. These materials have coercivity lying between 4 and 20 kA/m, and remanent flux density between 0.8 and 1.3 T. The program was developed (Appendix D) for PDP 1160 computer, and automatic plotting of B-H loop was carried out. It was observed that the intersection on the H-axis increases with the decrease in ratio of B_r/H_c. It was found that the maximum and minimum values of H_c critically determines the simulation of the loop. Comparison of the simulated B-H loops with those supplied from the permanent magnetic company show a very close agreement in all respect.

Based on parallelogram approximation of the B-H loop, the motor field equations were developed for the circumferential-flux type [8]. These equations were solved numerically to predict the terminal values of the motor. Using current as input, the airgap flux and hence line voltages are computed with the given stator windings. A complete computer algorithm is developed and the listings are included in Appendix E. The main computer program was first developed for IBM 360/55 systems. It was also made adoptable for PDP 1160 for integration with the graphic plotters.

The digital method of simulating the hysteresis loop and solving the motor equations numerically, allow the steady state behaviour of the hysteresis motor to be predicted from its known dimensions, winding data and hysteresis material's magneto-electric properties. The hysteresis ring of the test rotor was made of 17% cobalt steel alloys. The parallelogram approximation of the B-H loop is used in the numerical analysis of motor performance predictions. Test results of the terminal quantities at synchronous speed indicate good correlation between the measured and the calculated values.

Effects of pertinent hysteresis parameters like coercive force, remanentflux density, saturated relative permeability, and unsaturated relative permeability, on the airgap power of the hysteresis motor are studied.

The terminal properties of the hysteresis machine may be improved further by using the modified Frölich methods to solve the motor equations instead of the parallelogram. Developing a complete computer program in order to obtain, perhaps more accurate terminal quantities based on the modified Frölich model is one of the future works that should be carried out.

REFERENCES

1. Rahman, M.A., Gowda., S.D., "Representative Bibliography on Hysteresis Motors," IEEE Paper No. A79 071-2, IEEE PES Winter Meeting, New York, Feb. 04 - Feb. 09, 1979.

2. Helmic, C.G., Chapman, J.H., "The Modern Hysteresis Motor," Westinghouse Engineer, Vol. XXI, July, 1961, pp. 127-8.

3. Boehringer, A., "Electronic Hysteresis Motors for High Speed Rotor Drives," Elektrotechnik und Machinenbau, Vol. 87, No. 2, 1970, pp. 567-576.

4. Kenjo, T., "Speed Control of Hysteresis Synchronous Motors with 3-phase Transistor Invertor," IEE Conf. Publication No. 63, Conference on Electrical Variable Speed Drives, London, October 1972, pp.79-83.

5. Tanskii, E.A., "Automatic Speed Control System For a Hysteresis Motor," Izu. Vuz. Priborostr., No. 1, 1973, pp.44-48.

6. O'Kelly, D., "Hysteresis Motor with Solid State Control," IEE Conf. Publications, No. 136, March 1976, pp. 72-75.

7. Copeland, M.A., Slemon, G.R., "An Analysis of the Hysteresis Motor, I-Analysis of the Idealized Machine," IEEE Transactions, Vol. PAS-82, April 1963, pp. 34-42.

8. Copeland, M.A., Slemon, G.R., "An Analysis of the Hysteresis Motor, II-The Circumferential Flux Machine," IEEE Transactions, Vol. PAS-83, June 1964, pp. 619-625.

9. Steinmetz, C.P., "Theory and Calculation of Alternating Current Phenomena," (McGraw-Hill), N.Y., 1908, pp. 122 and 180.

10. Teare, B.R., "Theory of Hysteresis Motor Torque," AIEE Transactions, Vol. 59, 1940, pp. 907-912.

11. Roters, H.C., "The Hysteresis Motor, Advances Which Permit Economical Fractional hp Ratings," AIEE Transactions, Vol. 66, 1947, pp. 1419-1430.

12. Robertson, S.D.T., Zaky, S.Z.G., "Analysis of Hysteresis Machines Part I," IEEE Transactions, Vol. PAS-88, April 1969, pp. 474-483.

13. Miyairi, S., Kataoka, T., "A basic Equivalent Circuit of The Hysteresis Motor," JIEE, Vol. 85, 1965, pp. 41-50.

14. O'Kelly, D., "Equivalent Circuits for Single Phase Induction and Hysteresis Motors," IEEE Transactions, Vol. PAS-90, No. 1, 1971, pp. 279-288.

15. Rahman, M.A., "Analytical Models for Polyphase Hysteresis Motor," IEEE Transactions, Vol. PAS-92, No. 1, January/February 1973, pp. 237—242.

16. Das Gupta, A.K., "New Methods to Improve The Efficiency and Design of Hysteresis Motors," Journal Inst. of Eng. (India), Elec. Engineering Division, Vol.51, No. 10, Part EL-5, June 1971, pp. 268—281.

17. Morozov, G.G., "Designing Hysteresis Synchronous Motors for Minimum Power Consumption," Elektrichestvo, Vol. 10, 1967, pp. 36—39.

18. Slemon, G.R., Jackson, R.D., Rahman, M.A., "Performance Predictions for Large Hysteresis Motors," IEEE Transactions, Vol. PAS-96, Nov-Dec 1977, pp. 1915-1919.

19. Rahman, M.A., "Scale Modelling of Large Hysteresis Motors," IEEE Conf. Digest. Cat. No. 77 CHI 256-7, 1977, pp. 176—77.

20. Perard, J., Poloujadoff, M., "Study of Polyphase Hysteresis Motors With a Magnetic Ring of Medium Thickness," Revue Generale de L'electricite', Vol. 83, No. 2, Feb. 1974, pp. 71-75.

21. Rahman, M.A., Copeland, M.A., Slemon, G.R., "An Analysis of The Hysteresis Motor, III Parasitic Losses," IEEE Transactions, Vol. PAS-88, No. 6, June 1969, pp. 954-961.

22. Jackson, R.D., "Digital Simulation of The Hysteresis Motor," Proc. IEE, Vol. 120, No. 12, December 1973, pp. 1533-1537.

23. O'Kelly, D., "Hysteresis Motor With Overexcitation and Solid-state Control," Proc. IEE, Vol. 125, No. 4, 1978, pp. 288-292.

24. O'Kelly, D., "Theory and performance of Solid Rotor Induction and Hysteresis Machines," Proc. IEE, Vol. 123, No. 5, 1976, pp. 421—428.

25. Palli, L., Galan, N., "Magnetic Materials and Hysteresis Motor Performances," Electrotech. Electron and Autom. Electrotech (Rumania), Vol. 24, No. 2, Feb. 1976, pp. 71-5.

26. Potitsky, H., Butler, J.M. "A.C. Flux Penetration into Magnetic Materials With Saturation," Trans. IEEE (Communication and Electronics), Vol. 83, 1964, pp. 99—111.

27. Abrams, M.D., Gillot, D.H., "Numerical Analysis of Hysteresis and eddy Current losses in Solid cylindrical rods of No.1010 Steel," IEEE Transactions, Vol. PAS-86, No. 9, 1967, pp. 1077-1083.

28. Bullingham, J.M., Bernol, J.M., "Investigation of Non-linear B/H Loops on The Calculation of eddy Current Losses," Proc. IEE, Vol. 114, No. 8, 1967, pp. 1174-1176.

29. Zakrazewski, K., Pietras, F., "Methods of Calculating the Magnetic Field and Power Losses in Magnetic Materials, taking into account Magnetic Hysteresis," Proc. IEE, Vol. 118, No. 11, 1971, pp. 1679-1685.

30. Fisher, J., Moser, H., "The Reproduction of Magnetisation Curves by Simple Algebraic and Transcendental Functions," Archieve Elektrotechnik, Vol. 42, 1956, pp. 286-299.

31. Davis, N., "Derivation and Application of an Equation to the B-H Loop," J.Physics, D. Appl. Phys, Vol. 4, 1971, pp. 1034-1039.

32. Trutt, F.C., Erdely, E.A., Hopkins, R.E.," Representation of The Magnetisation Characteristics of d.c. Machine for Computer use," IEEE Transactions, Vol. PAS-87, No. 3, 1968.

33. Widger, G.F.T., "Representation of Magnetisation Curves Over Extensive Range by Rational Function Function Approximation," Proc. IEE, Vol. 116, 1969, pp. 156-160.

34. Macfaden, K.A., "Vector permeability," Journal IEEE, Vol. 94, Part 3, 1947, pp. 407-414.

35. Everatt, J.S., "Computer Simulation of Non-linear Inductors with Hysteresis," Electron Lett. No. 6, 1970, pp. 833-834.

36. Pearard, J., Poloujadoff, M., "Asynchronous Performance of Hysteresis Motors Under Unbalanced Condition," Electric Machines and Electromechanics, An International Quarterly, Vol. 1, No. 4, July-Sept. 1977, pp. 377-389.

37. Coulson, M.A., Slater, R.D., "Representation of Magnetic Characteristics Including Hysteresis, Using Preisach's Theory," Proc. IEE, Vol. 124, No. 10, October 1977, pp. 895-98.

38. Preisach, E., "On Magnetic After Effect," Z-Physics, 1935, pp. 277.

39. Neel's, L., "Theorie des lois d' Aimantafion de Lord Rayleigh," Cah. Phys, No. 12, Dec. 1942, pp. 1-20.

40. Biorci, G., Peseeti, D., "Mars 1968 Analytical Theory of The Behaviour of The Ferromagnetic Materials II Nuovo Cimento, Vol. VII., No. 6, pp. 828-842.

APPENDIX A

PREISACH-NÉEL'S MODEL

J. Perard and M. Poloujadoff [36] used this model in the study of the 'Asynchroronous performances of hysteresis motor under unbalanced conditions'. It seems to work very well for hysteresis materials like vicalloy. However, it is found that the modified Frölich approach gives a better B-H loop for materials like simonds-81 and Oerstit-70.

This model originates from a graphical representation of the hysteresis phenomenon given by Preisach [37, 38]. It is according to physical reality in low fields as shown by Néel [39] who gave a theory concerning the wall displacement in this case in 1942. Thus the name is Preisach-Néel's model.

Magnetisation curve of a Preisach-Néels elemental segment is shown in the Fig. (A1), by considering a small sample of magnetic material as the superposition of an arbitrary large number of elemental segments. Each one is characterized by two critical values of field intensity a and b ($a > b$) and has a rectangular hysteresis loop m(H) given in Fig. (A1). Each elemental segment is also represented in the (a, b) plane by a point below the first bisector ($a > b$) shown in Fig. (A2). If the intensity of the field sample is H, the magnetisation intensity of an elemental segment is given as:

$$m = M_s \text{ if } b < a < H \qquad (A1)$$

$$m = -M_s \text{ if } H < b < a \qquad (A2)$$

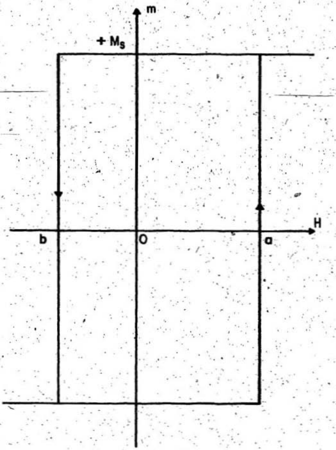

FIG. A1 MAGNETIZATION CURVE OF A PREISACH-NÉEL'S ELEMENTAL SEGMENT

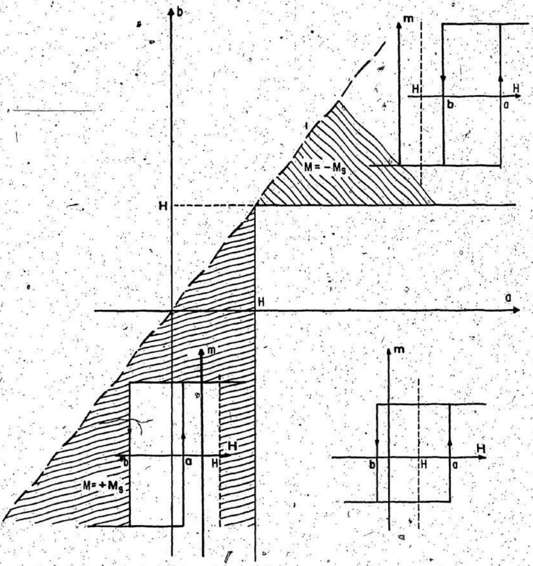

FIG. A2 PREISACH - NÉEL'S DIAGRAM

$$m = \pm M_s \text{ if } b \leq H \leq a \qquad (A3)$$

In the last case the sign of m is dependent on the previous history of the material. Therefore, the calculation must start from a state in which the value of m is known for all elemental segments.

Let 'n' be the total number of elemental segments in the sample. Then dn, the number of elemental segments having a representative point located in the rectangle defined by the coordinates (a, a + da, b, b + db). The M, the average value of m elemental segment

$$M = \frac{1}{n} \int_n m.dn \qquad \ldots\ldots\ldots\ldots (A4)$$

Next the model is completed by a distribution function S(a, b) related to the probability ($\frac{dn}{n}$) of finding an elemental segment having critical fields in the intervals (a, a + da) and (b, b + db). The function related to this is defined in the following way:

$$\frac{dn}{n} = \frac{1}{M_s} S (a, b) \, dadb \qquad \ldots\ldots\ldots\ldots (A5)$$

The magnetisation of the sample is given by

$$M = \int_{R^+} S (a, b) \, dadb - \int_{R^-} S (a, b) \, dadb. \quad (A5)$$

if R^+ and R^- are the regions of the (a, b) plane, where m is equal to $+ M_s$ and $- M_s$ respectively. Since the materials have the same properties, if all variations of H are changed in sign, S (a, b) is symmetrical with respect to the second bisector. In other words, S (a, b) = S (- b, - a). This function can be determined from the experimental knowledge of the rising magnetisation curve and the largest hysteresis cycle of the material. To determine the numerical values of S (a, b), the method proposed by Biorci and Pescetti [40] is used.

Based on the above principle J. Parard and M. Poloujadoff wrote a computer programme to compute the flux density $B = \mu_0 H + M$, knowing $H(t)$.
At the beginning the material is non-magnetised ($H = 0$, $M = 0$), the magnetised intensity of the elemental segment is given by the Fig. (A3a). Then

$m = S(a, b)$ below the second bisector,

$m = -S(a, b)$ above the second bisector,

$$\int_{R+} S(a, b)\,da\,db = \int_{R-} S(a, b)\,da\,db \quad \ldots\ldots (A6)$$

$$M(0) = 0 \quad \ldots\ldots\ldots\ldots\ldots\ldots (A7)$$

In a first stage, $H(t)$ increases from zero up to H_M. For a given value of H, m has changed from $-M_s$ into $+M_s$ for the elemental segments represented by points of the triangle T, Fig. (A3b). Thus:

$$M(t) = M(0) + 2\int_T S(a, b)\,da\,db \quad \ldots (A8)$$

Later M_M the final value of M, when $H = H_M$ (Fig. A3c) is called. Suppose in a second stage, $H(t)$ decreases from H_M, M decreases from M_M and is given by

$$M(t) = M_M - 2\int_{T_m} S(a, b)\,da\,db \quad \ldots\ldots (A9)$$

as long as $H > -H_M$ and H is steadily decreasing (Fig. A3d). If H reaches $-H_M$, Fig. (A3e) shows that M reaches $-M_M$. If H decreases further, $M(H)$ will be again the magnetisation curve. If, however, H increases again just after having reached H_M (with $H_M > -H_M$), M is given by:

$$M(t) = M_m + 2\int_{T_m} S(a, b)\,da\,db \quad \ldots\ldots (A10)$$

as long as $H < H_M$ and H is decreasing, Fig. (A3f).

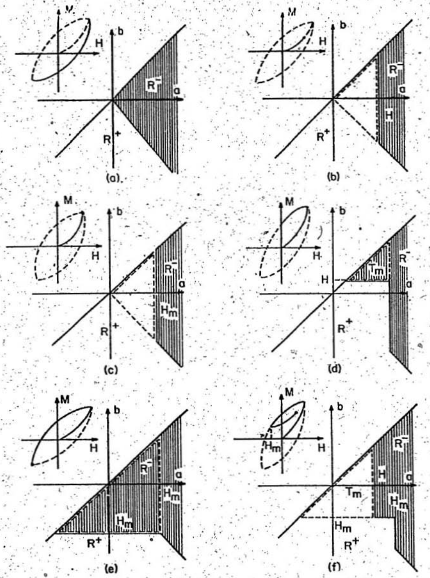

FIG. A3 ILLUSTRATION OF PREISACH – NÉEL'S MODEL

APPENDIX B

DESCRIPTION OF THE HYSTERESIS MOTOR UNDER STUDY

The stator of the hysteresis machine has a polyphase distributed winding. The rotor consists of a hysteresis ring supported by a aluminium sleeve. A hysteresis motor is a smooth cylindrical rotor electrical machine.

The Mawdsleys Generalised Machine is used in the experimental study. The stator of the experimental hysteresis motor is the stator of the Mawdsleys Generalised Machine. The stator of the Generalised Mawsleys Machine has a conventional 4-pole a.c winding in 48 slots. The ends of all the 48 coils are brought out to 96 terminals symmetrically arranged in four concentric circles. Thus, there is a unique flexibility of running the machine in several modes.

The arrangement of the physical relationship between the position of the coil sides and the arrangement of the terminals is shown in the adjoining photograph. Coil sides, 1-48 coloured red, are in slot position shown and the ends of these coil sides are connected to terminals 1-48, coloured red (not visible in the photopraph). Coil sides I-48, coloured blue are connected to terminals 1-48, coloured blue. The position of the slot numbers 1, 2, etc. are marked on the external connection plate.

There is a provision to measure the air gap flux, through the built in search coils, which is provided in the stator. Single search wires are provided in the tops of the stator slots 1, 7, 9, 12 and 13. The search coils of various pitches can be achived with this

EXPERIMENTAL MACHINE SET SHOWING DETAILS OF INSTRUMENTATION

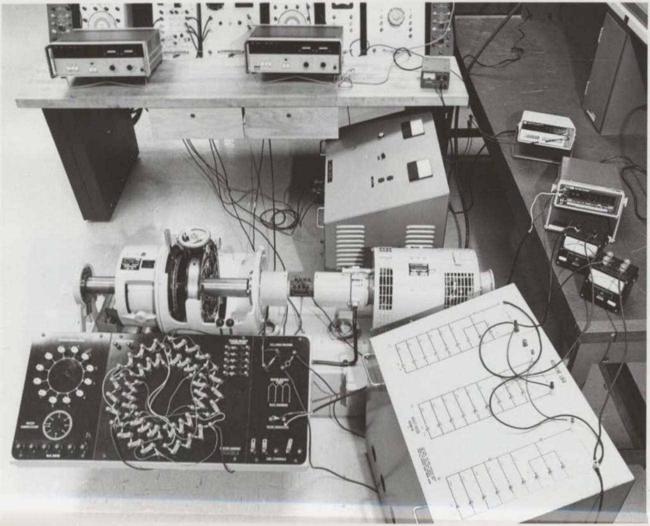

CLOSEUP VIEW SHOWING DETAILS OF WINDING CONNECTION

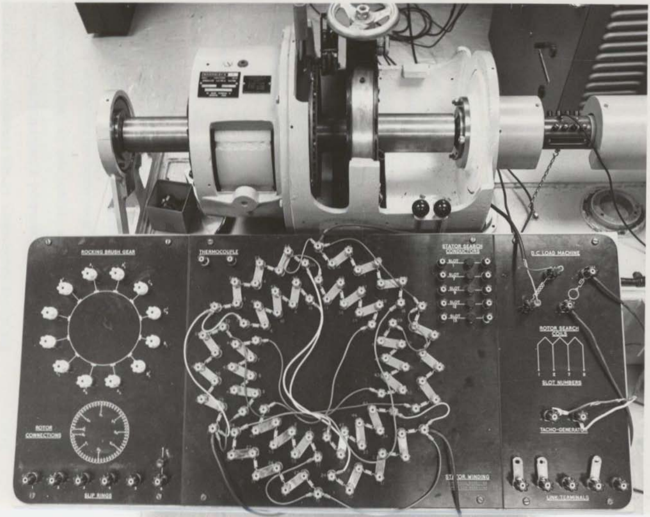

arrangement

The direct measurement of the temperature rise of the stator core is made possible by means of a built-in thermo couple. The ends of the thermo couple are brought out to the left-bottom corner of the connection plate. The insulation of the stator winding has a temperature tolerance limit of 110°C as measured by the thermocouple. The stator core temperature can also be measured with the help of a mercury thermometer, through a groove at the top of the stator core surface. The Mawdsleys Generalised Machine is coupled to a d.c work machine. The d.c work-machine is used to load the experimental hysteresis machine.

In addition a built-in a.c tacho-generator is provided for measuring the rotor speed, in the Generalised Machine set.

The torque measuring unit is the outstanding feature of the Generalised Machine set. The torque measuring unit facilitates accurate measurement of both steady state and transient torques. The torque to be measured is transmitted by a hollow shaft whose tapered end fits coaxially with the experimental rotor shaft, while the other end is coupled with the d.c work machine. The measured torque is to be obtained ultimately as an electrical output from the converter unit.

APPENDIX C

DESIGN DATA OF THE EXPERIMENTAL MACHINE

STATOR SPECIFICATIONS

The stator of the experimental hysteresis machine is the Mawdsleys Generalised Machine stator having the name plate data as follows.

Normal stator volts 200/220, stator No. 1

Stator core

Core material	Sheet steel 0.457 mm
Outside diameter	279.400 mm
Inside diameter	152.400 mm
Slot depth	27.080 mm
Slot width	2.540 mm
Tooth width	7.430 mm
Number of slots	48

Slots were tapered towards the air gap having 4.8 mm bottom radius and 2.8 mm tip radius.

Stator winding

Type of winding	douple layer lap
Number of coils	48
Number of conductors per slot	54
Number of turns per coil	27
Conductor dia	1.22 mm

Material	Copper
Mean length of turn	736.600 mm
Slot skew	1 slot pitch
Conductor covering	Polyvinyl acetate
Class of insulation	E

Rotor Specification

Diameter of the ring	151.250 mm
Outer diameter of the aluminium sleeve	118.500 mm
Ring depth	16.500 mm
Ring length	105.000 mm
Internal diameter of aluminium sleeve	97.400 mm
r_h of the sample	57.500 mm
r_g of the sample	67.560 mm
Shell thickness of sample	37.500 mm
Length of each sample	101.200 mm
Diameter of the shaft	75.500 mm
Air gap	0.508 mm
Stator resistance per phase	1.100 Ohm
Stator leakage reactance per phase	3.700 Ohm.

APPENDIX D

```
C          FILE NAME:      OST70.FTN
C          ************************************************
C          COMPUTER PROGRAMME TO SIMULATE THE B-H
C                  LOOPS OF THE HYSTERESIS MATERIALS LIKE
C                  17% COBALT STEEL, 36% COBALT STEEL AND
C                  OERSTIT-70 ( 16% COBALT STEEL ) ALLOYS.
C          ************************************************

C*************************************************************
C          SIMULATION OF OERSTIT-70 ALLOY IS
C                  GIVEN HERE AS AN EXAMPLE.
C*************************************************************
C
           COMMON/FUN/CA,BSAT,ALPHA
           DIMENSION H(128),B(128)
           CALL PLOTS(2)
           NEND=126
           DATA H/0.,500.,1000.,2000.,3000.,
           1 4000.,5000.,6000.,7000.,8000.,
           2 9000.,10000.,11000.,12000.,13000.,
           3 14000.,15000.,16000.,17000.,18000.,
           4 19000.,20000.,21000.,22000.,23000.,
           5 24000.,23000.,22000.,21000.,20000.,
           6 19000.,18000.,17000.,16000.,15000.,
           7 14000.,13000.,12000.,11000.,10000.,
           8 9000.,8000.,7000.,6000.,5000.,
           9 4000.,3000.,2000.,1000.,500.,
           1 0.,-500.,-1000.,-2000.,-3000.,
           2 -4000.,-5000.,-6000.,-7000.,-8000.,
           3 -9000.,-10000.,-11000.,-12000.,-13000.,
           4 -14000.,-15000.,-16000.,-17000.,-18000.,
           5 -19000.,-20000.,-21000.,-22000.,-23000.,
           6 -24000.,-23000.,-22000.,-21000.,-20000.,
           7  -19000.,-18000.,-17000.,-16000.,-15000.,
           8 -14000.,-13000.,-12000.,-11000.,-10000.,
           9 -9000.,-8000.,-7000.,-6000.,-5000.,
```

```
     1 -4000.,-3000.,-2000.,-1000.,-500.,
     2 0.,500.,1000.,2000.,3000.,
     3 4000.,5000.,6000.,7000.,8000.,
     4 9000.,10000.,11000.,12000.,13000.,
     5 14000.,15000.,16000.,17000.,18000.,
     6 19000.,20000.,21000.,22000.,23000.,
     7 24000.,0.,0./
       PI=4.*ATAN(1.)
       FMUO=4.*PI*1.0E-7
       FMURS=14.6
       ALPHA=FMUO*FMURS
       BSAT=1.2
       B(1)=0.
       HC=12500.
       CB=CONB(0.,0.,HC)
       CA=11.0E-4
       M=0
       DO 111 N=2,NEND
       B(N)=B(N-1)
       CALL FROLOP(H(N-1),B( N),H(N),M,HC,CB)
111    CONTINUE
D      WRITE(5,200)
200    FORMAT(/, ' MAGNETIC FIELD STRENGTH ',/)
       DO 5 K=1,NEND
5      H(K)=H(K)/1000.
D      WRITE (5,210) (H(K),K=1,NEND)
210    FORMAT (4F12.0)
D      DO 7 K=1,NEND
D7     B(K)=B(K)*10.
D      WRITE (5,230) (B(K),K=1,NEND)
D220   FORMAT (/, ' FLUX DENSITY ',/)
230    FORMAT (4F12.5)
       CALL AXIS (1.,5.,' ',-1,6.,0.,-30.,10.)
       CALL AXIS (4.,2.,' ',1,6.,90.,-1.5,.5)
       H(NEND+1)=-30.
       H(NEND+2)=10.
```

```
      B(NEND+1)=-1.5
      B(NEND+2)=.5
      CALL SYMBOL (1.,.9,.14,'FIG.(4.7). B-H LOOP FOR
     *OERSTIT-70 ( SIMULATED ).',0.,50)
D     CALL LINE (H,B,NEND,1,0,4,.14)
      CALL SPLINE(H,B,-NEND,1,0,32,0.)
      CALL PLEXIT
100   STOP
      END
      FUNCTION BXY(X,B)
      COMMON /FUN/CA,BSAT,ALPHA
      BXY=(CA*BSAT*X)/(1.+B*X)+(ALPHA*X)
      RETURN
      END
      FUNCTION CONB(U,V,W)
      COMMON /FUN/CA,BSAT,ALPHA
      CONB=(CA*BSAT)/(ABS(V)-ALPHA*(ABS(U)+W))-1./(ABS(U)+W)
      RETURN
      END
      FUNCTION YFX(X,Y,S,XX)
      YFX=(XX-X)*S+Y
      RETURN
      END
      FUNCTION ERR(X,Y,B)
      COMMON/FUN/CA,BSAT,ALPHA
      ERR=Y-((CA*BSAT*X)/(1.+B*X)+(ALPHA*X))
      RETURN
      END
      SUBROUTINE FROLOP(X,Y,XX,M,HC,CB)
      COMMON /FUN/CA,BSAT,ALPHA
      HCMIN=12500.
      HCMAX=12800.
      IF (M.EQ.-2) GO TO 90
      IF (M.EQ.2) GO TO 70
      IF (M.EQ.-1) GO TO 50
      IF (M.EQ.1)GO TO 30
```

```
C       DEAL WITH MODE M=0
        IF (XX-X) 11,12,13
13      YY=YFX(X,Y,ALPHA,XX)
        IF (YY) 14,15,15
14      XSTAR=-XX+HC
        YSTAR=-YY
        IF (XSTAR.LE.0.) GO TO 19
        ERRM2=ERR(XSTAR,YSTAR,CB)
        IF (ERRM2) 17,18,18
18      YSTAR=BXY(XSTAR,CB)
        Y=-YSTAR
        M=-2
        RETURN
19      XSTAR=XX-HC
        Y=BXY(XSTAR,CA)
        M=1
        RETURN
17      Y=YY
        M=0
        RETURN
15      XSTAR=XX-HC
        YSTAR=YY
        IF (XSTAR.LE.0.) GO TO 17
        ERR1=ERR(XSTAR,YSTAR,CA)
        IF (ERR1) 19,17,17
12      RETURN
11      YY=YFX(X,Y,ALPHA,XX)
        IF (YY) 20,21,21
20      XSTAR=-XX-HC
        YSTAR=-YY
        IF (XSTAR.LE.0.) GO TO 23
        ERRM1=ERR(XSTAR,YSTAR,CA)
        IF (ERRM1) 22,23,23
22      XSTAR=-XX-HC
        YSTAR=BXY(XSTAR,CA)
        Y=-YSTAR
```

```
      M=-1
      RETURN
23    Y=YY
      M=0
      RETURN
21    XSTAR=XX+HC
      YSTAR=YY
      IF (XSTAR.LE.0.) GO TO 22
      ERRM2=ERR(XSTAR,YSTAR,CB)
      IF (ERR2)23,26,26
26    Y=BXY(XSTAR,CB)
      M=2
      RETURN
C     MODE M=0 CALCULATIONS ARE COMPLETED
C     MODE M=1
30    IF (XX-X) 31,12,32
31    IF (ABS(Y)-BSAT) 40,41,41
41    HC=HCMAX
      GO TO 42
40    HC=HCMIN+(HCMAX-HCMIN)*ABS(Y)/BSAT
42    CB=CONB(X,Y,HC)
      IF (XX+HC) 33,34,34
33     XSTAR=-XX-HC
      YSTAR=BXY(XSTAR,CA)
      Y=-YSTAR
      M=-1
      RETURN
34    XSTAR=XX+HC
      Y=BXY(XSTAR,CB)
      M=2
      RETURN
32    XSTAR=XX-HC
      Y=BXY(XSTAR,CA)
      M=1
      RETURN
C     TRY MODE M=-1
```

```
50      IF (XX-X) 51,12,52
51      XSTAR=-XX-HC
        YSTAR=BXY(XSTAR,CA)
        Y=-YSTAR
        RETURN
52      IF (ABS(Y)-BSAT) 60,61,61
61      HC=HCMAX
        GO TO 62
60      HC=HCMIN+(HCMAX-HCMIN)*ABS(Y)/BSAT
62      CB=CONB(X,Y,HC)
        IF (XX-HC) 53,54,54
53      XSTAR=-XX+HC
        YSTAR=BXY(XSTAR,CB)
        Y=-YSTAR
        M=-2
        RETURN
54      XSTAR=XX-HC
        Y=BXY(XSTAR,CA)
        M=1
        RETURN
C       TRY WITH MODE M=2
70      IF (XX-X) 71,12,13
71      IF (XX+HC) 73,74,74
73      XSTAR=-XX-HC
        YSTAR=BXY(XSTAR,CA)
        Y=-YSTAR
        M=-1
        RETURN
74      XSTAR=XX+HC
        Y=BXY(XSTAR,CB)
        M=2
        RETURN
C       TRY WITH MODE =-2
90      IF (XX-X) 11,12,91
91      IF (XX-HC) 93,94,94
93      XSTAR=-XX+HC
```

```
      YSTAR=BXY(XSTAR,CB)
      Y=-YSTAR
      M=-2
      RETURN
84    XSTAR=XX-HC
      Y=BXY(XSTAR,CA)
      M=1
      RETURN
      END
```

APPENDIX E

FLOW DIAGRAM OF THE MOTOR EQUATION PROGRAM USED TO PREDICT THE TERMIAL PERFORMANCE OF HYSTERESIS MOTOR

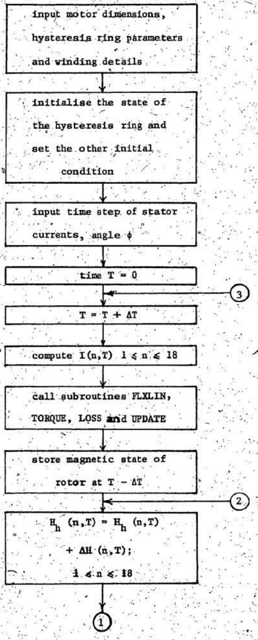

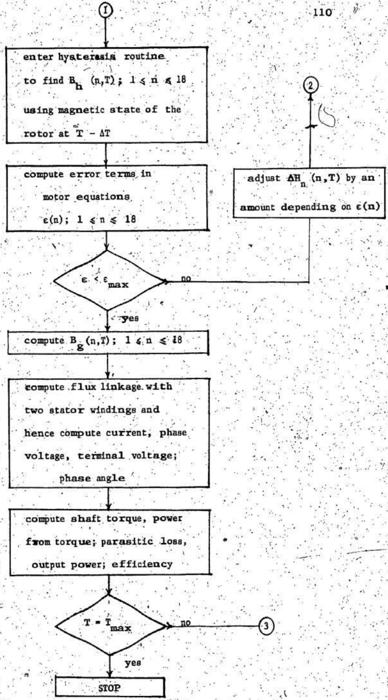
1
enter hysteresis routine to find $B_h(n,T)$; $1 \leq n \leq 18$ using magnetic state of the rotor at $T - \Delta T$
compute error terms in motor equations $\varepsilon(n)$; $1 \leq n \leq 18$
$\varepsilon < \varepsilon_{max}$
no
yes
2
adjust $\Delta H_n(n,T)$ by an amount depending on $\varepsilon(n)$
compute $B_g(n,T)$; $1 \leq n \leq 18$
compute flux linkage with two stator windings and hence compute current, phase voltage, terminal voltage; phase angle
compute shaft torque, power from torque; parasitic loss, output power; efficiency
$T = T_{max}$
no
3
yes
STOP

APPENDIX F

```
C       FILE NAME:      HYSMOT.FTN
C**************************************************************
C       COMPUTER PROGRAMME TO PREDICT THE TERMINAL
C            PERFORMANCE OF HYSTERESIS MOTOR.
C**************************************************************
        COMMON PI
        COMMON /GAP/RO,ALPHA,BETA,TOP,BOT,EF,RIG,PX,QX,RX,SX,TX,UX,VX,WX
        COMMON /CURR/FM,FIP,VHBP,VHCP,REL,VHB,VHC,ARC,MODE,MODEP
        COMMON /FLUX/VOLTSP,NT,DAREA,PSI,FIG
        COMMON /POWER/VH,FI,TORQ,VOL
        COMMON /PARAS/GAPDIA,CONLOS,PLOSS
        COMMON /WIND/WINDIN,DTHETA,PHI,FREQ,PP
        DIMENSION FI(36),FM(18),FIG(36)
        DIMENSION FIP(18),VHBP(18),VHCP(18),MODEP(18)
        DIMENSION VHB(18),VHC(18),MODE(18),VH(36),VHSCAL(18)
D       DIMENSION NINCA(8),STACRA(8),PHIA(8)
        DIMENSION NINCA(3),STACRA(3),PHIA(3)
        PI=4.*ATAN(1.)
        GAPDIA=160.5/1000.
        AIR GAP=.508/1000.*1.
        RING=16.30/1000.
        RINDIA=GAPDIA-RING
        RINWID=100.10/1000.
        FMUO=4.*PI/10.0E6
        PP=2.
        DTHETA=PI/(18.*PP)
        REL=(2.*AIRGAP*RING)/(FMUO*GAPDIA*DTHETA)
        CONTF=(2.*RING)/(GAPDIA*DTHETA)
        ARC=RINDIA*DTHETA/2.
        DAREA=RINWID*GAPDIA*DTHETA/2.
        VOL=PI*RINDIA*RING*RINWID
        WRITE (5,801)
801     FORMAT (/,'   CIRCUMFERENTIAL FLUX MACHINE PARAMETERS' ,/)
        WRITE (5,802) GAPDIA,RINDIA
802     FORMAT (9H GAP DIA=,E10.4,1HM,10H RING DIA=,E10.4,1HM)
        WRITE (5,803) RING,RINWID
```

```
803     FORMAT (12H RING DEPTH=,E10.4,1HM,7H WIDTH=,E10.4,1HM)
        WRITE(5,804) AIRGAP
804     FORMAT (8H AIR GAP=,E10.4,1HM)
C       SETUP WINDING PARAMETERS
        WINDIN=27.*12.*1.732/(PI*PI)
        SLOTS=48.
        FREQ=60.
        RES=1.1
        X1R=3.7
        WRITE (5,852) WINDIN,RES,X1R
852     FORMAT (16H WINDING FACTOR=,F7.3,5H OHMS,25H  STATOR
     *PHASE RESISTANCE=,F5.3,3H OH,7H REACT=,F5.3)
        WRITE (5,853) SLOTS,PP,FREQ
853     FORMAT (21H  TOTAL NO. OF SLOTS=,F6.3,F6.3,11H POLE PAIRS,
     *19H  SUPPLY FREQUENCY=,F5.1,5H HERZ)
        FMURS=10.
D       TYPE *,'FMURS'
D       ACCEPT *,FMURS
        FMURO=100.
D       TYPE *,'FMURO'
D       ACCEPT *,FMURO
        RESIST=.28E-6
        ALPHA=FMURS*FMUO
        BETA=FMURO*FMUO
        RO=400.
        TOP=.8
D       TYPE *,'TOP'
D       ACCEPT *,TOP
        RIG=9500.
D       TYPE *,'RIG'
D       ACCEPT *,RIG
        WRITE (5,881)
881     FORMAT (/,'   HYSTERESIS RING PARAMETERS',/)
        WRITE (5,882) FMURS,FMURO,TOP,RIG
882     FORMAT (8H MU SAT=,F5.1,11H  MU UNSAT=,F5.1,
     *11H  BR (REM)=,F4.2,6H TESLA,4H HC=,E10.3,4H A/M)
```

```
      WRITE(5,883) RESIST
883   FORMAT (18H RING RESISTIVITY=,E10.2,6H OHM-M)
      W=PI/10.
      BOT=-TOP
      EF=-RIG
      PX=-(TOP+BETA*RIG)/(BETA-ALPHA)
      WX=-PX
      SX=(TOP-BETA*RIG)/(BETA-ALPHA)
      TX=-SX
      RX=-(TOP+BETA*(RIG-RO))/(BETA-ALPHA)
      UX=-RX
      QX=RX-RO
C     INITIALISE THE HYSTERESIS RING AND CALCULATE
C     THE LOSS EXPRESSION FACTORS
      DO 160 J=1,18
      VH(J)=0.
      FI(J)=0.
      VHB(J)=-RO
      VHC(J)=RO
      MODE(J)=0
160   CONTINUE

      BETA1=SQRT(.5*(-1.+SQRT(1.+(CHI**4))))
      ETA1=.98
      A1=.43
      CONLOS=(DAREA*GAPDIA*FREQ*PI*BETA1*A1*A1*ETA1*ETA1)/(2.*ALPHA)
      NSTART=1
      DATA NINCA/10,10,10/
D     DATA STACRA/7.24,5.31,8.23/
D     DATA STACRA/8.23,9.27,10.17/
D     DATA STACRA/10.86,10.82,9.31/
D     DATA STACRA/9.39,9.18,9.7/
D     DATA STACRA/9.84,9.92,10.29/
D     DATA STACRA/10.37,10.49,10.82/
D     DATA STACRA/10.86,10.94,10.9/
D     DATA STACRA/10.9,10.98,11.06/
```

```
      DATA STACRA/8.,7.8,7.9/
      DATA PHIA/0.,0.,0./
      NNN=3
      DO 1000 III=1,NNN
      NINC=NINCA(III)
      STACUR=STACRA(III)
      PHI=PHIA(III)
      NEND=NSTART+NINC
      FMP=STACUR*WINDIN*3./2.
C     BASIC COMPUTATION LOOP TO DETERMINE THE B AND H
C     IN THE HYSTERESIS RING AT SUCCESSIVE INTERVALS
      DO 65 NT=NSTART,NEND
      T=NT
      DO 2 J=1,18
      SEG1=J
      FM(J)=FMP*DTHETA*PP*SIN(W*T-PP*SEG1*DTHETA-PHI)
100   FIP(J)=FI(J)
      VHBP(J)=VHB(J)
      VHCP(J)=VHC(J)
      MODEP(J)=MODE(J)
2     CONTINUE
201   CALL UPDATE
65    CONTINUE
      NT=NEND
      FIG(1)=(FI(2)+FI(18))*CONTF/2.
      DO 7 J=2,17
      FIG(J)=(FI(J+1)-FI(J-1))*CONTF/2.
7     CONTINUE
      FIG(18)=(-FI(1)-FI(17))*CONTF/2.
      CALL FLXLIN
      CALL TORQUE(PP)
      CALL LOSS
      PSIDEG=PSI*180./PI
      PHIDEG=PHI*180./PI
      VINPH=(VOLTSP+STACUR*RES*COS(PSI))+STACUR*X1R*SIN(PSI)
      VOUTPH=(STACUR*X1R*COS(PSI)-STACUR*RES*SIN(PSI))
```

```
      VCOMP=SQRT(VINPH*VINPH+VOUTPH*VOUTPH)
      VRMS=VCOMP/1.414
      CURRMS=STACUR/1.414
      POW1=TORQ*FREQ*2.*PI/PP
      POW2=3.*VOLTSP*STACUR*COS(PSI)/2.
      PERR=(POW1-POW2)*100./POW1
      POW3=3.*RES*STACUR*STACUR/2.
      POW4=POW1-PLOSS
      EFF=POW4*100./(POW1+POW3)
      WRITE (5,711) NT,STACUR,PHIDEG
711   FORMAT (//12H  TIME STEP=,I3,27H  STATOR CURRENT AMPLITUDE=,
     *F8.2,1HA,15H   FLUX ANGLE=,F7.2,3HDEG)
      WRITE (5,712) VOLTSP,PSIDEG,VCOMP
712   FORMAT (/16H  AIR GAP VOLTS=,F8.2,2H V,16H AT PHASE ANGLE=,
     *F9.2,14H   TERM.VOLTS=,F8.2,2H V)
      WRITE (5,713) TORQ,POW1
713   FORMAT (/9H  TORQUE=,E10.4,4H N-M,20H  POWER FROM TORQUE=,
     *E10.4,6H WATTS)
      WRITE(5,714) POW2,PERR
714   FORMAT (21H  (3*V*I*COS(PSI))/2=,E10.4,6H WATTS
     *8H  ERROR=,F7.2,1H%)
      WRITE (5,715) POW3,PLOSS
715   FORMAT(/25H  STATOR RESISTANCE LOSS=,E10.4, 6H WATTS,
     *17H  PARASITIC LOSS=,E10.4,6H WATTS)
      WRITE (5,716) POW4,EFF
716   FORMAT (/15H  OUTPUT POWER=,E10.4,6H WATTS,
     *13H  EFFICIENCY=,F6.1,1H%)
      WRITE (5,12)
12    FORMAT (31H  AIR GAP FLUX DENSITY IN WB/M2)
      WRITE (5,13)  (FIG(J),J=1,18)
13    FORMAT (9F8.4/9F8.4)
      WRITE (5,14)
14    FORMAT (19H  HYST FLUX DENSITY)
      WRITE(5,15) (FI(J),J=1,18)
15    FORMAT (9F8.4/9F8.4)
      DO 152 J=1,18
```

```
      VHSCAL(J)=VH(J)/1000.
152   CONTINUE
      WRITE (5,150)
150   FORMAT (/29H  HYST MAGNETIC FIELD IN KA/M)
      WRITE (5,151) (VHSCAL(J),J=1,18)
151   FORMAT (9F8.3/9F8.3)
      NSTART=NEND
1000  CONTINUE
      STOP
      END
C     'UPDATE' CALCULATES HYSTERESIS RING FLUX DENSITY
C     AND MAGNETIC FIELD STRENGTH FOR EACH SEGMENT OF THE RING.
C     CALLS ON SUBROUTINE LOOP
      SUBROUTINE UPDATE
      COMMON PI
      COMMON /GAP/RO,ALPHA,BETA,TOP,BOT,EF,RIG,PX,QX,RX,SX,TX,UX,VX,W
      COMMON /CURR/FM, FIP,VHBP,VHCP,REL,VHB,VHC,ARC,MODE,MODEP
      COMMON /POWER/VH,FI,TORQ,VOL
      DIMENSION FI(36),FM(18),VH(36),VHB(18),VHC(18),MODE(18)
      DIMENSION FIP(18),VHBP(18),VHCP(18),MODEP(18)
      DIMENSION ERROR(18),FIDIST(18)
      EPSIL=RIG/1000.
      VHINC=RIG/10.
D     TYPE *,'TEST',ARC
16    J=1
      MC=0
17    N=1
1701  IF (J.EQ.1) GO TO 1702
      IF (J.EQ.18) GO TO 1703
      FIDIST(J)=2.*FI(J)-FI(J-1)-FI(J+1)
      GO TO 1706
1702  FIDIST(1)=2.*FI(1)+FI(18)-FI(2)
      GO TO 1706
1703  FIDIST(18)=2.*FI(18)-FI(17)+FI(1)
1706  ERROR(J)=(VH(J)-(FM(J)-REL*FIDIST(J))/ARC)
      IF (ABS(ERROR(J))-EPSIL) 18,18,18
```

```
18      MC=MC+1
        IF (MC.EQ.18) GO TO 1930
1800    IF (J.EQ.18) GO TO 1920
        J=J+1
        GO TO 17
19      SG=SIGN(1.,ERROR(J))
1902    IF  (N.EQ.1) GO TO 1910
        IF (SSG*SG) 1800,1800,1910
1910    VH(J)=VH(J)-SG*VHINC
        FI(J)=FIP(J)
        VHB(J)=VHBP(J)
        VHC(J)=VHCP(J)
        MODE(J)=MODEP(J)
        CALL LOOP (VH(J),FI(J),VHB(J),VHC(J),MODE(J))
        SSG=SG
        N=N+1
        GO TO 1701
1920    VHINC=VHINC*.66
        GO TO 16
1930    RETURN
        END
        FUNCTION XFY(X,Y,S,YY)
        XFY=(YY-Y)/S+X
        RETURN
        END
        FUNCTION YFX (X,Y,S,XX)
        YFX=(XX-X)*S+Y
        RETURN
        END
C       SUBROUTINE FLXLIN FIRST CALCULATES THE FLUX LINKED
C       WITH A SINGLE TURN COIL WITH SIDES AT J AND J+18,
C       AND THEN ADDS THE CONTRIBUTION OF A SET OF COILS TO
C       FROM THE TOTAL FLUX LINKED WITH TWO ORTHOGONAL COILS
C       FROM THESE THE PEAK PHASE VOLTS AND PHASE ANGLE
C       ARE FOUND
        SUBROUTINE FLXLIN
```

```
      COMMON PI
      COMMON /FLUX/VOLTSP, NT, DAREA, PSI, FIG
      COMMON /WIND/WINDIN, DTHETA, PHI, FREQ, PP
      DIMENSION FIG(36), FL(36)
      DO 4 J=19,36
      FIG(J)=-FIG(J-18)
4     CONTINUE
      DO 1 K=1,18
      FL(K)=0.
      KEND=K+18
      DO 2 J=K,KEND
      FL(K)=DAREA*FIG(J)+FL(K)
2     CONTINUE
1     CONTINUE
      FLA=0.
      FLB=0.
      CON=WINDIN*DTHETA*PP
      DO 3 J=1,18
      SEG=J
      FLA=CON*SIN(SEG*DTHETA*PP)*FL(J)+FLA
      FLB=CON*COS(SEG*DTHETA*PP)*FL(J)+FLB
3     CONTINUE
      VOLTSA=FLA*FREQ*2.*PI*PP
      VOLTSB=FLB*FREQ*2.*PI*PP
      VOLTSP=SQRT(VOLTSA*VOLTSA+VOLTSB*VOLTSB)
      T=NT
      WT=T*PI/10.
      ANG=0.
      IF (VOLTSB) 10,15,7
7     IF (VOLTSA) 9,9,11
9     ANG=PI
10    ANG=ANG+PI
11    PSID=ATAN(VOLTSA/VOLTSB)
12    PSI=PSID-WT+ANG+PHI
      IF (PSI) 13,14,14
13    PSI=PSI+2.*PI
```

```
14    RETURN
15    PSID=PI-SIGN(CPI/2.), VOLTSA)
      ANG=PI
      GO TO 12
      END
      SUBROUTINE TORQUE(POLPAR)
C     'TORQUE' CALCULATES THE HYSTERESIS LOOP AREA
C     FORMED BY THE B-H DISTRIBUTION IN THE RING
      COMMON PI
      COMMON /POWER/VH,FI,TORQ,VOL
      DIMENSION VH(36),FI(36)
      DO 4 J=19,36
      VH(J)=-VH(J-18)
      FI(J)=-FI(J-18)
4     CONTINUE
      TORQ=POLPAR*VOL*(VH(1)-VH(36))*(FI(1)+FI(36))/(4.*PI)
      DO 1 J=2,36
      TORQ2=(VH(J)-VH(J-1))*(FI(J)+FI(J-1))/(4.*PI)
      TORQ=TORQ+POLPAR*VOL*TORQ2
1     CONTINUE
      RETURN
      END
C     'LOOS' ESTIMATES PARASITIC LOSS IN THE
C     HYSTERESIS RING WHEN THE MOTOR IS IN
C     THE REGION OF SYNCHRONISM. INCLUDES FLUX
C     PARASITIC LOOS ONLY
      SUBROUTINE LOSS
      COMMON /WIND/WINDIN,DTHETA,PHI,FREQ,PP
      COMMON /PARAS/GAPDIA,CONLOS,PLOSS
      COMMON /FLUX/VOLTSP,NT,DAREA,PSI,FIG
      DIMENSION FIG(36)
      PLOSS=0.
      DO 1 J=1,36
      PLOSS=PLOSS+CONLOS*FIG(J)*FIG(J)
1     CONTINUE
      RETURN
```

```
      END
C     SUBROUTINE LOOP IS PARALLELOGRAM MODEL OF THE
C     HYSTERESIS LOOP INCLUDING MINOR, RECOIL, LOOPS
      SUBROUTINE LOOP (X,Y,B,C,M)
      COMMON PI
      COMMON /GAP/RO,ALPHA,BETA,TOP,BOT,EF,RIG,PX,QX,RX,SX,TX,UX,VX,W
      IF (M.GE.2) GO TO 41
      IF (M.LE.-2) GO TO 51
C     AT FIRST DEALS WITH MODES -1,0,AND 1 ONLY
      IF (X.LT.B) GO TO 36
      IF (X.LT.C) GO TO 35
      IF (M.NE.-1) GO TO 34
31    IF (X.LT.VX) GO TO 33
      IF (X.LT.WX) GO TO 32
      Y=YFX(0.,TOP,ALPHA,X)
      B=X
      C=X
      M=4
      RETURN
32    Y=YFX(RIG,0.,BETA,X)
      C=X
      B=XFY(0.,TOP,ALPHA,Y)
      M=3
      RETURN
33    Y=YFX(RIG,0.,BETA,X)
      C=X
      B=X-RO
      M=-1
      RETURN
34    D=(Y-ALPHA*C+BETA*RIG)/(BETA-ALPHA)
      IF (X.GT.D) GO TO 31
      Y=YFX(C,Y,ALPHA,X)
      C=X
      B=X-2.*RO
      B1=XFY(EF,0.,BETA,Y)
      IF (B.GT.B1) GO TO 340
```

```
      B=B1
340   M=0
      RETURN
35    RETURN
36    IF (M.NE.1) GO TO 40
37    IF (X.GT.QX) GO TO 39
      IF (X.GT.PX) GO TO 38
      Y=YFX(0.,BOT,ALPHA,X)
      B=X
      C=X
      M=-4
      RETURN
38    Y=YFX(EF,0.,BETA,X)
      B=X
      C=XFY(0.,BOT,ALPHA,Y)
      M=-3
      RETURN
39    Y=YFX(EF,0.,BETA,X)
      B=X
      C=X+RO
      M=1
      RETURN
40    A=(Y-ALPHA*B+BETA*EF)/(BETA-ALPHA)
      IF (X.LT.A) GO TO 37
      Y=YFX(B,Y,ALPHA,X)
      B=X
      C=X+2.*RO
      C1=XFY(RIG,0.,BETA,Y)
      IF (C.LT.C1) GO TO 400
      C=C1
400   M=0
      RETURN
C     DEALS WITH MODES 2,3 AND 4
41    IF (X.LT.B) GO TO 46
      IF (M.NE.4) GO TO 43
42    Y=YFX(0.,TOP,ALPHA,X)
```

```
      B=X
      C=X
      M=4
      RETURN
43    IF (X.LT.C) RETURN
      IF (M.NE.3) GO TO 45
44    IF (X.GT.WX) GO TO 42
      Y=YFX(RIG,0.,BETA,X)
      C=X
      B=XFY(0.,TOP,ALPHA,Y)
      M=3
      RETURN
45    IF (X.GT.VX) GO TO 44
      Y=YFX(C,Y,ALPHA,X)
      C=X
      B=X-RO
      RETURN
46    IF (X.GT.WX) GO TO 42
      IF (X.GT.UX) GO TO 50
      IF (X.GT.SX) GO TO 49
      IF (X.GT.QX) GO TO 48
      IF (X.GT.PX) GO TO 47
      Y=YFX(0.,BOT,ALPHA,X)
      B=X
      C=X
      M=-4
      RETURN
47    Y=YFX(EF,0.,BETA,X)
      B=X
      C=XFY(0.,BOT,ALPHA,Y)
      M=-3
      RETURN
48    Y=YFX(EF,0.,BETA,X)
      B=X
      C=X+RO
      M=1
```

```
      RETURN
49    Y=YFX(0.,TOP,ALPHA,X)
      B=X
      C=X+RO
      M=2
      RETURN
50    Y=YFX(0.,TOP,ALPHA,X)
      B=X
      C=XFY(RIG,0.,BETA,Y)
      M=3
      RETURN
C     DEALS WITH MODES -2,-3 AND -4
51    IF (X.LT.B) GO TO 56
      IF (M.NE.-4) GO TO 511
      IF (X.LT.PX) GO TO 58
510   IF (X.LT.RX) GO TO 55
      IF (X.LT.TX) GO TO 54
      IF (X.LT.VX) GO TO 53
      IF (X.LT.WX) GO TO 52
      Y=YFX(0.,TOP,ALPHA,X)
      B=X
      C=X
      M=4
      RETURN
511   IF (X.GT.C) GO TO 512
      RETURN
512   GO TO 510
52    Y=YFX(RIG,0.,BETA,X)
      C=X
      B=XFY(0.,TOP,ALPHA,Y)
      M=3
      RETURN
53    Y=YFX(RIG,0.,BETA,X)
      C=X
      B=X-RO
      M=-1
```

```
      RETURN
54    Y=YFX(0.,BOT,ALPHA,X)
      C=X
      B=X-RO
      M=-2
      RETURN
55    Y=YFX(0.,BOT,ALPHA,X)
      C=X
      B=XFY(EF,0.,BETA,Y)
      M=-3
      RETURN
56    IF (M.EQ.-4) GO TO 58
      IF (M.EQ.-3) GO TO 57
      IF (X.GT.QX) GO TO 60
57    IF (X.GT.PX) GO TO 59
58    Y=YFX(0.,BOT,ALPHA,X)
      B=X
      C=X
      M=-4
      RETURN
59    Y=YFX(EF,0.,BETA,X)
      B=X
      C=XFY(0.,BOT,ALPHA,Y)
      M=-3
      RETURN
60    Y=YFX(B,Y,ALPHA,X)
      B=X
      C=X+RO
      RETURN
      END
```